AN ATMOSPHERIC SENSITIVITY AND VALIDATION STUDY OF THE VARIABLE TERRAIN RADIO PARABOLIC EQUATION MODEL (VTRPE)

THESIS

Matthew K. Doggett, Captain, USAF

AFIT/GM/ENP/97M-04

DEPARTMENT OF THE AIR FORCE
AIR UNIVERSITY
AIR FORCE INSTITUTE OF TECHNOLOGY

Wright-Patterson Air Force Base, Ohio

AFIT/GM/ENP/97M-04

AN ATMOSPHERIC SENSITIVITY AND VALIDATION STUDY OF THE VARIABLE TERRAIN RADIO PARABOLIC EQUATION MODEL (VTRPE)

THESIS

Matthew K. Doggett, Captain, USAF

AFIT/GM/ENP/97M-04

The views expressed in this thesis are those of the author and do not reflect the official policy or position of the Department of Defense or the U. S. Government.

AFIT/GM/ENP/97M-04

AN ATMOSPHERIC SENSITIVITY AND VALIDATION STUDY OF THE VARIABLE TERRAIN RADIO PARABOLIC EQUATION MODEL (VTRPE)

THESIS

PRESENTED TO THE FACULTY OF THE GRADUATE SCHOOL OF ENGINEERING
OF THE AIR FORCE INSTITUTE OF TECHNOLOGY
AIR UNIVERSITY
AIR EDUCATION AND TRAINING COMMAND
IN PARTIAL FULFILLMENT OF THE REQUIREMENTS FOR THE DEGREE OF MASTER OF SCIENCE IN METEOROLOGY

MATTHEW K. DOGGETT, B. S.
CAPTAIN, USAF

MARCH 1997

AFIT/GM/ENP/97M-04

AN ATMOSPHERIC SENSITIVITY AND VALIDATION STUDY OF THE VARIABLE TERRAIN RADIO PARABOLIC EQUATION MODEL (VTRPE)

MATTHEW K. DOGGETT, B. S.
CAPTAIN, USAF

Approved:

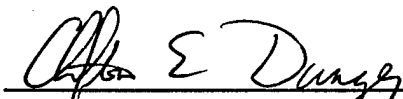

CLIFTON E. DUNGEY, Major
Committee Chairman

10 MAR 97
Date

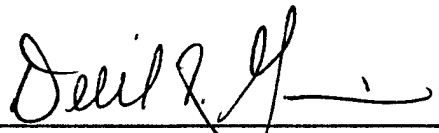

DERRILL T. GOLDIZEN, Major
Committee Member

10 Mar 97
Date

DAVID R. WOOD, Captain
Committee Member

10 Mar 97
Date

Acknowledgments

I wish to extend my gratitude to several people who contributed time and thoughts to help me in the completion of this thesis. Major Pat Hayes, Captain Dave Wood, and Captain John Polander all assisted in the launch of several radiosondes used in part of this paper. Major Jason Tuell provided helpful insights after reading a very rough draft of this report. Glenn Hunter from Penn State graciously provided the MM5 data. Finally, thanks go to my thesis advisor Major Cliff Dungey for making this thesis experience...well...for making this a thesis experience I'll not likely forget in a lifetime.

My wonderful wife Sherry and daughter Kiersten were as always a source of blessing and encouragement to a husband and father who was exceedingly busy during the long months preparing this report. I owe them much for their invaluable support.

Table of Contents

List of Figures

List of Tables

Abstract

The Variable Terrain Radio Parabolic Equation (VTRPE) computer model is a powerful and flexible program that provides calculations of the radar propagation conditions of the atmosphere. It is limited however, by the accuracy and resolution of the input data. This study quantifies the sensitivity of the VTRPE model to the accuracy and resolution of the atmospheric parameters that go into it. Also, two case studies are examined to test the utility of VTRPE in operational use.

The sensitivity to measurements of pressure, temperature, and humidity was found to be dependent on the meteorological environment. In standard and subrefractive environments, average values of Root Mean Squared Error in calculating propagation pathloss were greatest for measurement errors in humidity. While the overall RMSE averaged only 0.5% to 5%, in certain regions the errors in calculating pathloss were as high as 20%.

VTRPE was used to calculate possible height errors when birds were detected at long ranges from a WSR-88D radar in a ducting environment. While the radar assumes a standard atmosphere when calculating height, results from VTRPE suggest that this resulted in possible height errors of over 3 km. Another case study of detected anomalous propagation was examined to determine the effects of multiple soundings in the VTRPE calculation of propagation pathloss. In this example, the effect of assuming a homogeneous atmosphere resulted in propagation pathloss errors of up to 30%.

AN ATMOSPHERIC SENSITIVITY AND VALIDATION STUDY OF THE VARIABLE TERRAIN RADIO PARABOLIC EQUATION MODEL

Chapter 1. Introduction

Many are familiar with the optical illusions caused by the bending of visible light as it travels through very strong vertical gradients of temperature ($^{dT}/_{dz}$). Mirages and heat shimmering are common occurrences in arid, desert climates. Also, the scattering of extra-terrestrial light passing through the entire depth of the atmosphere is known to cause stars to twinkle in the night sky. This bending phenomena is not limited only to the visible wavelengths of electromagnetic energy but extends into the VHF radio and radar frequencies as well. This phenomenon is known as refraction and its effects on radar and radio wave propagation have been observed since the early 1940's (Ko, et al. 1983; Rogers 1996).

a. Background

The use of radar and radio communications is a vital component of successful military operations. Air traffic control, search radars, guided weapons, and airborne radar control all make use of radio wave propagation through the atmosphere to send and receive information. Unfortunately, at the frequencies that these systems operate, atmospheric conditions are not transparent to the passage of the electromagnetic wave. It

is in the microwave region (VHF to K_u-band) of 100 MHz to 30 GHz that variations in the tropospheric refractivity field can have dramatic effects (Ko et al., 1983).

Most operational systems designers typically assume meteorological conditions of a range-independent, "standard atmosphere" where the temperature decreases with height at a rate of approximately 6.5 °C km^{-1} and humidity is constant (see Appendix B). However, the atmosphere is frequently non-standard and certainly can vary over the horizontal path of propagation. In the vicinity of frontal boundaries, near thunderstorms, under clear skies at night, and in many other situations, the temperature and moisture profiles differ from this standard condition. Most of the time this results in small or unnoticeable variations in electromagnetic path propagation. However, in some cases the difference between non-standard and standard atmospheric conditions on the path of a radio or radar beam can be dramatic. This "anomalous propagation" (AP) is defined as "the abnormal bending and diversion of electromagnetic radiation from intended paths, resulting in problems with coverage fading, height errors, and anomalous clutter" (Schemm et al., 1987). Ryan (1991b) has noted three reasons for this deviation from standard conditions:

1. Reflection and scattering off the earth's surface.
2. Earth curvature and terrain cast a shadow causing diffraction.
3. Variations in the atmospheric refractive index causes bending and reflection of energy.

It is for these reasons that numerous attempts have been made to model the effects of the atmosphere on electromagnetic wave propagation.

b. Literature Review

Initial efforts at propagation modeling described the path of a radar beam as a single ray. Using geometric optics and Snell's Law, one could describe the path this ray of energy would take through the atmosphere. With the advent of computer technology, many scientists have written computer programs that model radio wave propagation. One program widely used by military agencies has been the Integrated Refractive Effects Prediction System (IREPS) originally described by Hitney and Richter (1976). However, this program was designed for use aboard naval ships and did not account for horizontal variations in the atmosphere or terrain.

More recently, a number of models based upon the parabolic wave approximation (see Appendix A) have been developed to offer a more complete picture of tropospheric wave propagation. The Electromagnetic Parabolic Equation (EMPE) model developed by Johns Hopkins Applied Physics Lab is able to describe detailed features of propagation loss due to anomalous tropospheric refraction (Ko et al., 1983). The EMPE program allows for greater flexibility in describing the environment and the antenna patterns used in propagation calculations (Dockery and Konstanzer, 1987). Schemm et al. (1987) used a numerical model of the atmospheric boundary layer to provide the refractivity estimates to be used in EMPE to generate propagation path loss diagrams. In 1989, a parabolic equation model for personal computers (PEPC) was developed and used as part of a technique to model propagation in range-dependent environments (Barrios, 1992).

With all these recent advances, few studies addressed the sensitivity of propagation models to the meteorological parameters that go into them. Helvey (1983) revealed that

the measurement error of radiosondes introduces a false bias toward refractive duct occurrences that can lead to erroneous propagation model calculations. Cook (1991) evaluated the sensitivity of several evaporation duct height algorithms to atmospheric parameters. In 1996, Rogers used the Radio Physical Optics (RPO) program to examine the errors introduced with the assumption of a horizontally homogeneous troposphere.

The latest generation of propagation models include terrain effects in the calculation of electromagnetic wave propagation. Ryan (1991a, 1991b) developed a computer program designed to model range-dependent, tropospheric microwave propagation that accounts for variable surface terrain and meteorological conditions. This Variable Terrain Radio Parabolic Equation (VTRPE) model will be the focus of this study.

c. VTRPE

The VTRPE program is a full-wave, propagation physics computer model that predicts the path a radar or radio wave will travel through an atmosphere that is both vertically and horizontally variant. It accepts one or more atmospheric refractivity profiles as meteorological input and generates a range-height diagram of propagation pathloss of radar energy in decibels (dB). In addition, it has the following characteristics (Ryan, 1991b):

1. infinite or finite conductivity surface boundary conditions
2. Linear transmitter polarization (vertical or horizontal)
3. variable surface terrain elevation and dielectric properties
4. frequency dependent atmospheric attenuation
5. transmitter frequency range from 0.1 to 30 GHz

6. generalized transmitter antenna radiation patterns

d. Problem Statement

This model has promise for operational use in predicting communications and radar coverage patterns for any terrain and meteorological conditions. However, effective use of the VTRPE model depends heavily upon accurate meteorological measurements and forecasts of a sufficient resolution to capture the variability of an inhomogeneous atmosphere.

The only meteorological input required by the VTRPE model is one or more vertical refractivity profiles. Measurement of refractivity values typically comes from the measurements of temperature, pressure, and humidity (see Chapter 2) from the worldwide network of radiosonde upper-air observing sites. Current vertical resolution of these reported atmospheric soundings is coarse. The horizontal resolution is even worse due to the limited number of these observing sites.

Before wide-scale development and operational use of the VTRPE model can continue, it is important to quantify the sensitivity of this model to measurement errors and resolution of current observational and forecasting systems. The objective of this study is twofold:

1. To determine the sensitivity of VTRPE to meteorological inputs, and,
2. To validate observed cases of anomalous radar signatures during ducting conditions with the results predicted by VTRPE.

In reaching these objectives the author will attempt to answer the following questions:

1. How do changes in horizontal and vertical resolution of data change the results computed by VTRPE?

2. Does the VTRPE model correctly identify anomalous propagation conditions as observed on a meteorological radar?

3. How can VTRPE assist in determining height errors in an AP environment?

Chapter 2. Tropospheric Refraction

a. Refractivity

The phenomena of refraction and anomalous propagation are best understood from the concept of a unitless parameter called the index of refraction. Commonly named the refractive index of a medium, n is given by the ratio of the speed of light in a vacuum, c, to the speed of light in the medium, v (Battan, 1977):

$$n = \frac{c}{v}. \tag{1}$$

The speed of light in the medium is calculated from Maxwell's equations and is always less than the speed of light in free space. Thus the refractive index exceeds the value of unity throughout the troposphere[1]. For convenience purposes, refractive index is often given in terms of refractivity N,

$$N = (n-1)\times 10^6. \tag{2}$$

Bean and Dutton (1966) have shown that at microwave frequencies, N is related to the measured atmospheric variables of temperature, pressure, and humidity. This empirical relationship is

$$N = \frac{77.6}{T}\left(p + 4810\frac{e}{T}\right) \tag{3}$$

where temperature (T) is in Kelvin, pressure (p) and vapor pressure (e) are in hPa and N is unitless.

[1] The value of n used for the near-earth atmosphere is usually 1.0003.

Equation 1 shows that an increase (decrease) in refractivity corresponds to a decrease (increase) in the speed of light in the medium. Thus, we would expect that gradients of N would result in the bending of electromagnetic waves as the velocity with which they travel through the atmosphere changes. These variations in refractivity are common in the non-homogeneous troposphere, where there are both vertical and horizontal gradients of temperature, pressure, and moisture. In most cases, the horizontal variations of N are so small that only the vertical variations of refractivity are considered when describing the propagation of electromagnetic energy through the atmosphere (Bean and Dutton 1966). However, this assumption of horizontal homogeneity is not valid where strong horizontal variations are known to exist (e.g., across a sea-breeze or extra-tropical frontal boundaries).

Figure 1 shows the variation of refractivity with height in a standard atmosphere with different degrees of relative humidity. Under these conditions, N is approximately 300 at the surface and decreases with height since pressure, temperature, and vapor pressure also decrease with height. The gradient of N is greatest at lower elevations where the magnitude of temperature, pressure, and vapor pressure is greatest. Also, the effect of increasing humidity is to increase the vertical gradient of N. The reason for this is the refractivity dependence on temperature and vapor pressure. The Clausius-Clapeyron equation given by

$$\frac{de_s}{e_s} = \frac{L}{R_v}\frac{dT}{T^2} \tag{4}$$

relates the saturation vapor pressure (e_s) to temperature (Wallace and Hobbs, 1977; Fleagle and Businger, 1980). As the temperature increases, the vapor pressure increases

exponentially. Consequently, the contribution of vapor pressure to the calculation of refractivity increases and is greatest near the earth's surface.

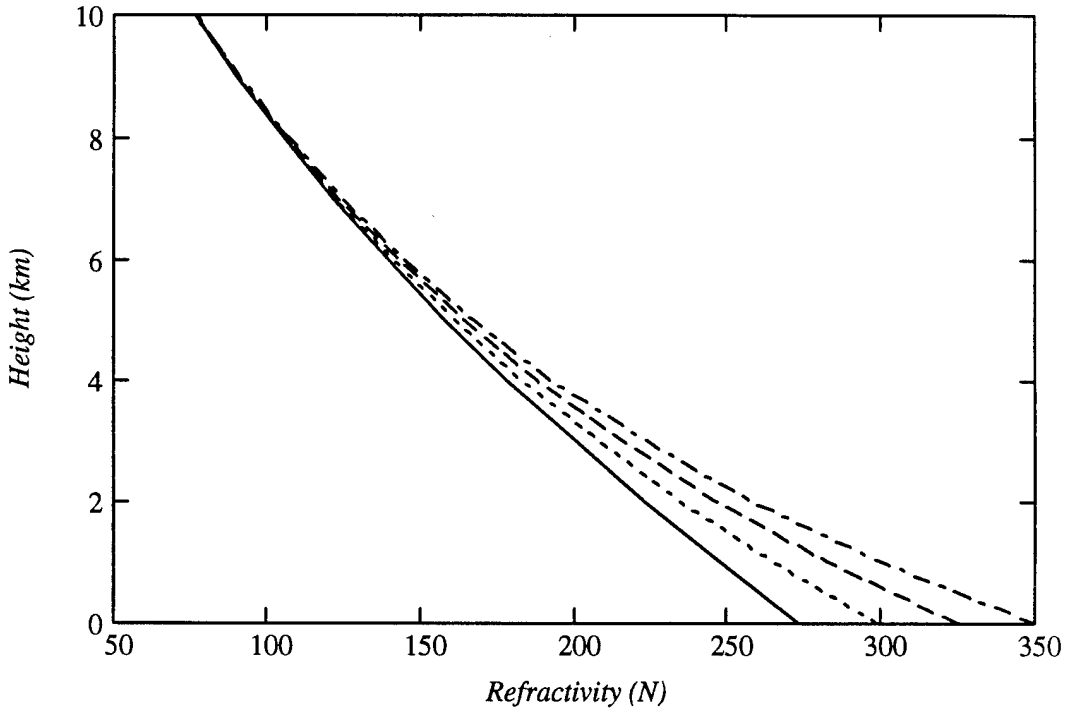

Figure 1. Vertical distribution of refractivity for the standard atmosphere. Solid line represents a dry atmosphere, dotted (RH=33%), dashed (RH=67%), dash-dot (RH=100%).

This is evident in Figure 2, which shows how N varies with temperature and humidity at a constant pressure level (p = 1000 hPa). At temperatures below freezing, there is very little change in refractivity values between a dry and saturated environment. This is why AP caused by humidity induced refractivity variations are relatively rare in cold environments. As the temperature increases, the saturation vapor pressure of the atmosphere increases dramatically. This greatly enhances the refractivity gradient across moisture boundaries thus creating a more favorable environment in which AP might occur.

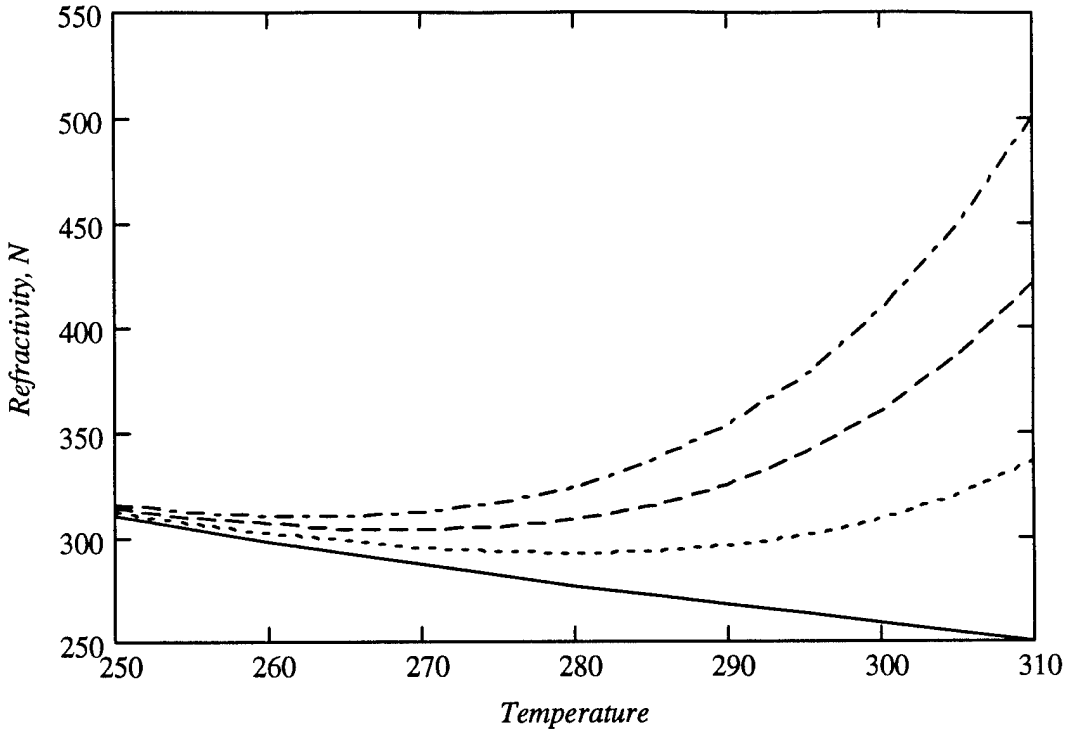

Figure 2. The dependence of refractivity on temperature and humidity at 1000 hPa (adapted from Ko et al. 1983). Solid line represents dry atmosphere, dotted (RH=33%), dashed (RH=67%), dash-dot (RH=100%).

b. Ducting, Super-refraction, and Sub-refraction

As noted previously, the electromagnetic propagation state of the atmosphere is generally described by the vertical variations in refractivity. Under standard atmospheric conditions (Figure 1), the vertical gradient of N in the lower troposphere (0-1 km) is a value between -54 N km^{-1} (100% relative humidity) and -25 N km^{-1} (dry atmosphere)[2]. This decrease in N with height corresponds to a gradual increase in the speed of light according to Equation 1. Therefore, under standard atmospheric conditions, a beam of

[2] The most commonly used standard atmosphere refractivity value is -39 N-units km^{-1} which corresponds to a humidity of approximately 50% through the depth of the troposphere.

electromagnetic energy propagating through a standard atmosphere tends to be "bent" downward towards the earth's surface (Figure 3).

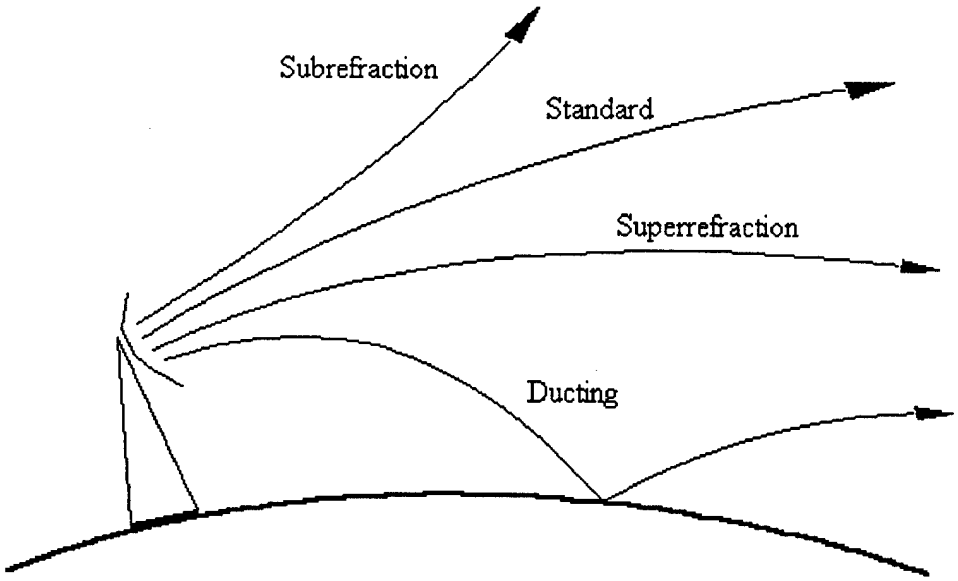

Figure 3. Classification of Propagation conditions in the Troposphere.

Propagation environments other than standard are classified either as super- or subrefractive. Subrefractive conditions occur for refractivity gradients less than standard (e.g., $dN/dz = -20$ N km^{-1}) and the ray of energy is bent less than normal. Superrefraction occurs when the downward bending of these rays is greater than normal. This occurs when $dN/dz < -54$ N km^{-1}.

Ducting is an extreme case of superrefraction when the energy ray is bent so much that it actually becomes trapped between a layer in the atmosphere and the earth's surface. This is known as a surface, or evaporation, duct and occurs for gradients where $dN/dz < -157$ N km^{-1} at the earth's surface. Ducting can also occur in an elevated layer

where the beam is trapped between two layers of atmosphere. Ducting is the most extreme case of anomalous wave propagation and also causes the greatest deviation from normal refractive conditions (Figure 3).

It is easiest to visualize ducting conditions through the use of another common unit describing the refractivity conditions of the atmosphere. The modified refractive index, M, takes into account both the propagation of the wave of energy and the curvature of the earth. It is given by,

$$M = N + \left(h/a\right) \cdot 10^6 \tag{5}$$

where h is the height of the electromagnetic wave above the earth's surface and a is the earth radius. The advantage of this unit is that atmospheric ducts are easily recognized when the gradient of M is negative. Figure 4 shows idealized M profiles for three types of propagation ducts. In an evaporation duct, the M profile decreases with height from the earth's surface to the top of the duct. In a surface-based duct, the lowest value of M, which defines the top of the duct, is less than the value of M at the surface. The surface of the earth is the bottom boundary of the ducting layer. The elevated duct is bounded on the top and bottom by the atmosphere. The duct thickness is the height difference between the top of the duct and the lower level where the value of M equals the value of M at the top of the duct.

Table 1 summarizes the four types of propagation environments and the commonly used values of refractivity and modified refractivity units for each.

Table 1. Summary of atmospheric propagation environments and their associated refractivity gradients.

Propagation Environment	N-gradient, dN/dz ($N\ km^{-1}$)	M-gradient, dM/dz ($M\ km^{-1}$)
Standard Atmosphere		
Rel. Humidity=0%	-25	+132
Rel. Humidity=50%	-39	+118
Rel. Humidity=100%	-54	+111
Subrefractive	greater than -25	greater than +132
Superrefractive	-54 to -157	+111 to 0
Ducting	less than -157	less than 0

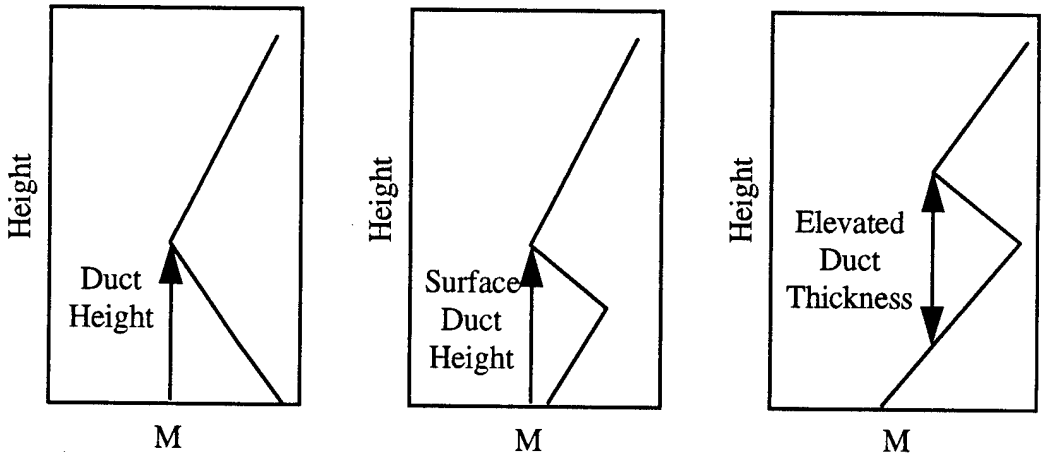

Figure 4. Idealized M profiles for an evaporation, a surface-based, and an elevated atmospheric propagation duct.

c. Meteorological Conditions Favorable for Duct Formation

As stated above, ducting conditions arise from rapid decreases in refractivity with height. From Equation 3 we see that rapid *decreases* in vapor pressure, or rapid *increases* in temperature support this type of scenario. Meteorologically, the most common situation for these to occur simultaneously is in a temperature inversion. Inversions are an important source of ducting conditions for two reasons: stability and persistence (Bean

and Dutton, 1966). Stability is important because it inhibits turbulent mixing in the lower troposphere and allows strong vertical gradients of humidity to develop if there is a source of significant moisture at the surface. This is one reason why a large number of ducting phenomena occur in a maritime environment. Secondly, inversions are commonly associated with slowly moving regions of high pressure that dominate the weather pattern over large regions. This is significant in that favorable ducting conditions can affect a large area for a significant period of time.

Temperature inversions can result from one of four processes: advection, radiation, subsidence, and in a thunderstorm downdraft.

Advection. The flow of dry, warm air over a cool, moist surface creates both temperature and moisture gradients that are key to duct formation.

Radiation. Clear skies and light surface winds at night assist in the radiational cooling of the earth's surface. Evaporation and surface based ducts are usually a result of this mechanism. However, if the air cools enough so that fog occurs, the latent heat of condensation is added to the air. Thus, the temperature gradients are reduced and this helps to inhibit the creation of a duct.

Subsidence. The downward motions associated with upper atmospheric ridges and surface high pressure cause the air to be heated by adiabatic compression. This warm, dry air settles over large regions of cool, moist air at the surface. This situation is most common in the formation of elevated ducts.

Thunderstorm downdraft. The precipitation associated with thunderstorms and strong rain showers creates a pool of descending air that is much cooler than the

surrounding environment. This can result in a temperature inversion in the lower elevations as this cooler air spreads out beneath the base of the storm. Although sharply defined cases that result in AP are relatively rare, they are important because of its proximity to the storm.

Though these conditions for temperature inversions and duct formation can occur any time of the year and in any location, the most common environment for duct formation is a maritime environment during the summer months. High moisture content near the surface with very warm surface temperatures capped by drier, cooler air are the key ingredients for AP conditions.

d. Errors in the measurement of N

Accurate measurement of pressure, temperature, and moisture content is critical for precise calculation of refractivity in Equation 3. Assuming that this formula for N is exact, an expression for errors in N given independent errors in pressure, temperature, and moisture is given by,

$$\delta N = \frac{\partial N}{\partial p}\delta p + \frac{\partial N}{\partial T}\delta T + \frac{\partial N}{\partial e}\delta e \tag{6}$$

where δp, δT, and δe represent small changes or errors in measurement of pressure, temperature, and vapor pressure (Bean and Dutton, 1966). Equation 6 can be written as

$$dN' = c_1\Delta p + c_2\Delta T + c_3\Delta e \tag{7}$$

where c_1, c_2, and c_3 are the partial derivatives of Equation 3 evaluated in reference to a standard atmosphere. A root-mean-square error for N is then given by

$$\Delta N = \left[(c_1\Delta p)^2 + (c_2\Delta T)^2 + (c_3\Delta e)^2\right]^{1/2}. \tag{8}$$

Typical values for constants c_1, c_2, and c_3 for a standard atmosphere with 60% relative humidity are listed in Table 2. The magnitude of c_3 indicates that the measurement of vapor pressure contributes more to the error of calculating N than either pressure or temperature. Considering the strong temperature dependence of vapor pressure, one concludes that the measurement error of refractivity is also strongly dependent on temperature.

Table 2. Values of the constants c_1, c_2, and c_3 in Equation 7 and 8 for a standard atmosphere of 60% relative humidity.

Altitude (Km)	N	P (hPa)	T (K)	e (hPa)	c_1 (hPa^{-1})	c_2 (K^{-1})	c_3 (hPa^{-1})
0	319	1013	288.15	10.3	0.269	-1.27	4.50
1	279	898	282.65	6.7	0.276	-1.10	4.71
2	244	790	275.15	4.3	0.282	-0.96	4.93
4	186	602	262.15	1.4	0.296	-0.73	5.43
6	141	445	249.15	0.42	0.312	-0.57	6.01
8	105	318	236.15	0.11	0.329	-0.45	6.69
10	76	219	223.15	0.02	0.348	-0.34	7.50

Figure 5 shows the calculation error of N in a standard atmosphere and 60% relative humidity where the measurement errors for a typical radiosonde are ± 1 hPa pressure (δp), ± 0.5 K temperature (δT), and ± 3% relative humidity (proportional to δe). Calculated errors are greatest in the lowest altitudes of the profiles and decrease with height. This reflects the fact that the temperature and vapor pressure are greatest near the surface and decrease with height. Also, calculation errors increase significantly when temperature profiles are warmer than "standard". In an atmosphere that is uniformly 20 degrees warmer than standard, errors in measuring refractivity are more than twice that of a standard atmosphere. The error in calculating N at high altitudes (e.g., above 8 km) is

negligible compared lower elevations regardless of temperature. These features arise from the strong temperature dependence of vapor pressure.

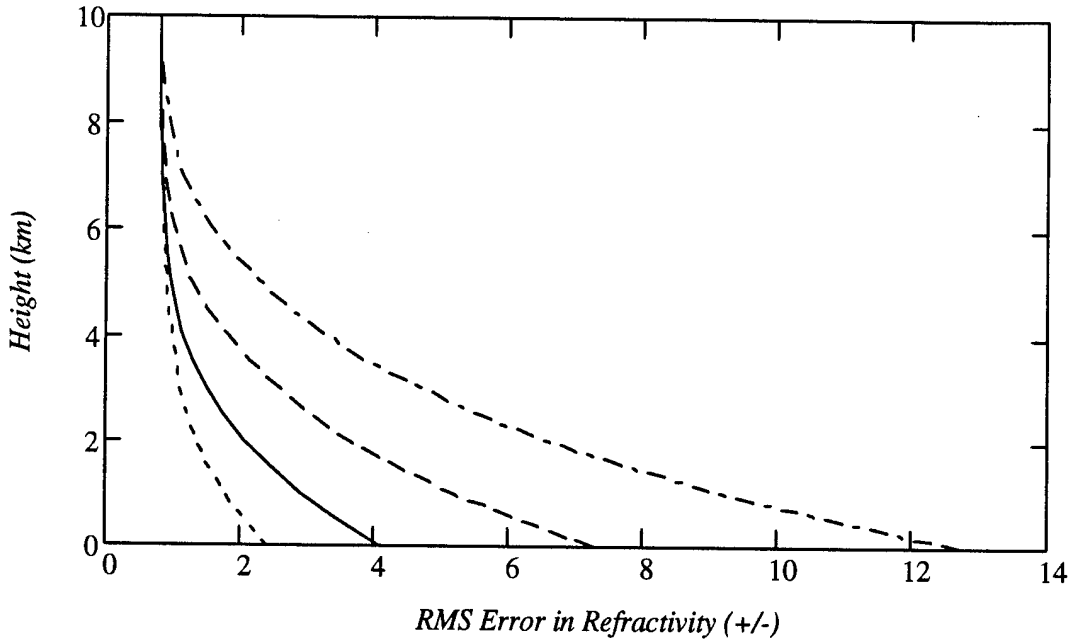

Figure 5. RMS Error in calculating refractivity for a standard atmosphere profile at 60% relative humidity. Solid line represents standard atmosphere, dotted (10 K colder than standard), dashed (10 K warmer than standard), dot-dashed (20 K warmer).

Chapter 3. Methodology

The method of study is divided into two parts. The first is to determine the sensitivity of VTRPE to meteorological inputs. The second is to compare observed cases of anomalous radar signatures during ducting conditions with the results predicted by VTRPE.

a. Sensitivity to meteorological inputs

The only meteorological input required by the VTRPE model is the vertical refractivity profile. Measurement of refractivity values typically comes from the measurements of temperature, pressure, and humidity (see Chapter 2) from the worldwide network of radiosondes. Therefore, the accuracy of VTRPE forecasts of radio propagation is ultimately limited by the accuracy with which the meteorological parameters are measured by a radiosonde and the vertical resolution or sampling rate of the instrument. The former is a function of the type of sensors used on the radiosonde and is relatively consistent worldwide. The latter however, is generally at the mercy of each individual operator who determines when the radiosonde records an observation, often based upon a predetermined set of meteorological criteria.

This study is an effort to quantify the sensitivity of VTRPE to the accuracy and resolution of these measured atmospheric quantities. The former requires that the meteorological variables be measured with a small enough error that the model is able to produce meaningful results. The latter condition requires that the input data be of

sufficient resolution that the horizontal and vertical variations of the atmosphere are captured.

1) ACCURACY

The objective here was to determine, quantitatively, how much the VTRPE output changes due to variations in the refractivity profile. First, an S-band (~3 GHz) WSR-88D radar was modeled using VTRPE and a standard atmosphere refractivity profile. The VTRPE model produced a 200 x 100 grid (range vs. height) diagram of one-way pathloss (in dB) of radar energy. Because the majority of refractive effects on radar propagation are limited to the lower elevations and to speed computer processing, the model domain was limited to 2 km in altitude and 200 km in range.

Second, to simulate the measurement error of a radiosonde, random errors were introduced to each of the meteorological parameters: pressure (p), temperature (T), and relative humidity (RH) which go into calculating refractivity in Equation 3. Five different values of maximum random error were introduced into each of these variables both independently and simultaneously. These five error levels represent the range of error common in many of the radiosonde instruments used today and are listed in Table 3. For each level of error, thirty "error" profiles were generated to provide a statistical sample of a population representing the results from a typical radiosonde launch. The VTRPE program used each of these profiles as input to create radar coverage diagrams of propagation pathloss. The results from the "error-free" standard atmosphere profile were compared to the results from each of the "error" profiles by computing a relative pathloss uncertainty ($\Delta\beta$) at each of the gridpoints in the range-height grid,

$$\Delta\beta_i = \left[\left(\frac{\beta_i - \beta_{oi}}{\beta_{oi}}\right)^2\right]^{1/2} \tag{9}$$

where β represents the pathloss value at the gridpoint for the "error" atmosphere, and β_o represents the "error-free" pathloss value. The average of $\Delta\beta$ over the entire region is a type of normalized root mean squared error (RMSE) where

$$RMSE = \sqrt{\frac{1}{M}\sum_{i=1}^{M}\left(\frac{\beta_i - \beta_{oi}}{\beta_{oi}}\right)^2} \tag{10}$$

and M is the number of grid points (Wilks, 1995). This value of RMSE is normalized with respect to the original field so that it represents a percent error from the undeviated coverage diagram.

Table 3. Levels of error represent the maximum error introduced into the atmospheric parameters that go into calculating refractivity. Errors are randomly determined to be positive or negative.

Error Level	Pressure (hPa ±)	Temperature (K ±)	Relative Humidity (% ±)
1	0.5	0.2	1
2	1.0	0.5	2
3	1.5	1.0	3
4	2.0	1.5	4
5	2.5	2.0	5

This same procedure of generating a simulated environment, creating random deviations from it, and comparing the original to the deviations will be done for the four cases of:

1. standard atmosphere (dM/dz = 111-132 $M\ km^{-1}$),
2. subrefractive atmosphere (dM/dz > 132 $M\ km^{-1}$),

3. atmosphere with an elevated duct, and,
4. atmosphere with an evaporation duct.

(i) Standard atmosphere

The standard atmosphere in Figure 6 represents an atmosphere at 50% relative humidity. Temperature and dewpoint decrease at a nearly constant rate and the modified refractivity increases at a rate of approximately 117-128 M km^{-1}. Specific details in calculating a standard atmosphere are described in Appendix B.

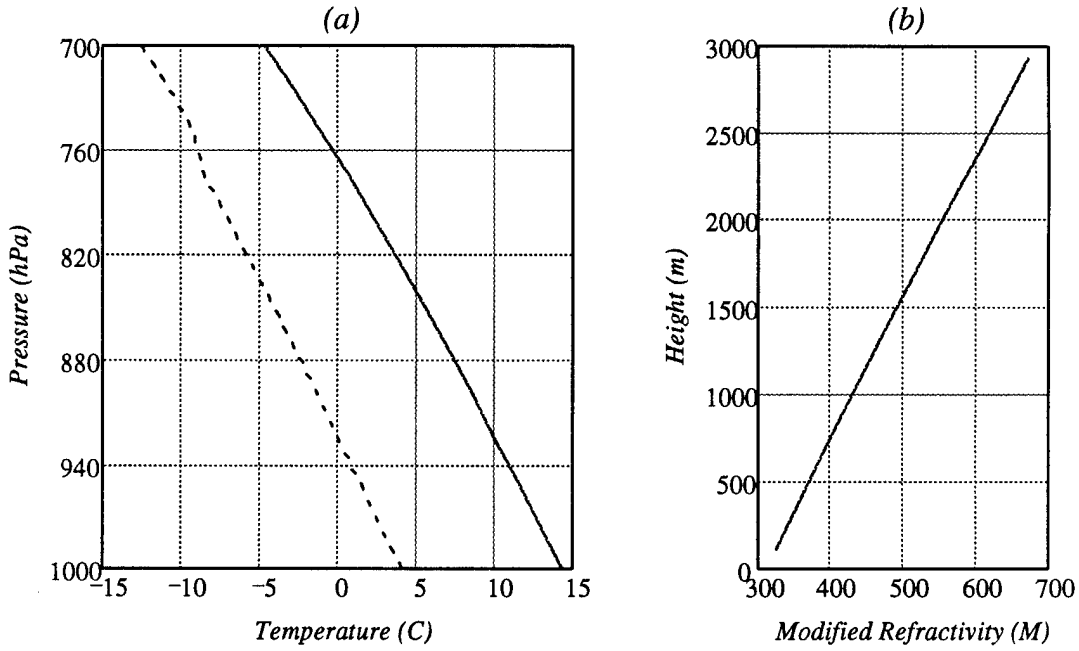

Figure 6. Radiosonde (a) and modified refractivity (b) profiles of a standard atmosphere at 50% relative humidity. In (a): solid line is temperature, dotted line is dewpoint.

(ii) Subrefractive atmosphere

The subrefractive atmosphere shown in Figure 7 is common in a very dry regime where the temperature lapse rate is nearly dry adiabatic and humidity increases with

height. Under these conditions, temperature decreases at a nearly constant rate while the dewpoint is constant or may increase slightly with height. This results in a modified refractivity profile that increases at a rate of approximately 140 M km^{-1}. This type of profile, common in the High Plains and the western mountain regions of the U.S., is called a Type IV, "inverted V" sounding (Bluestein, 1993) and is occasionally associated with severe convection.

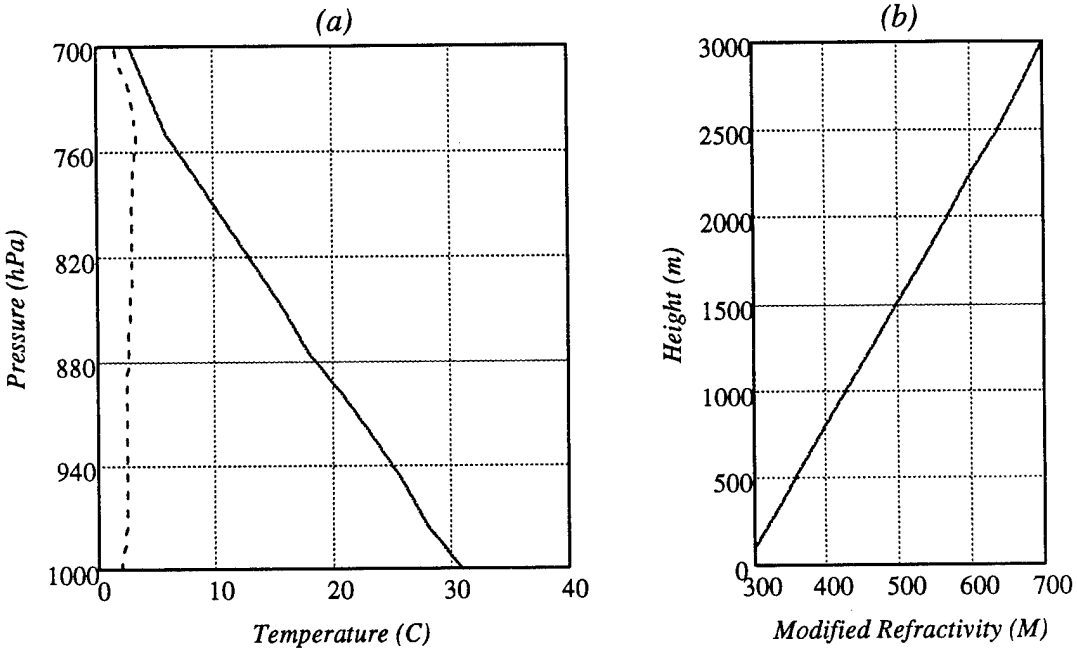

Figure 7. Radiosonde (a) and modified refractivity (b) profiles of a subrefractive atmosphere. In (a): solid line is temperature, dotted line is dewpoint.

(iii) Elevated duct

Figure 8 shows representative profiles of a marine inversion layer typically found along the California coastline. Such a profile has a very strong, moist inversion layer just above the surface which is capped by a layer of dry air aloft. This type of sounding

produces a refractivity profile that initially is positive, but in the inversion layer it decreases with height resulting in an elevated propagation duct. In this example the top of the elevated duct is at 550 m.

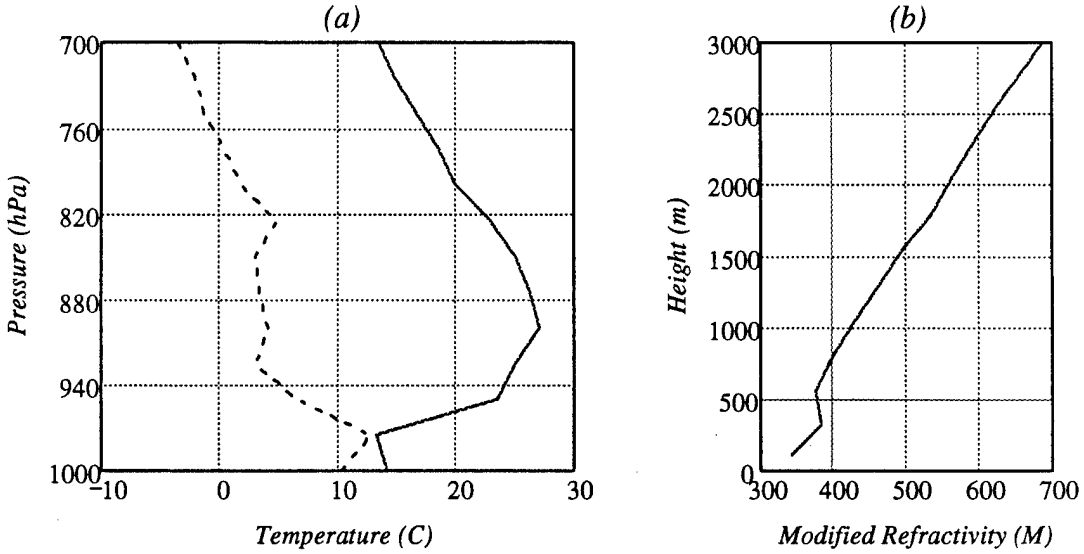

Figure 8. Radiosonde (a) and modified refractivity (b) profiles of an atmosphere with an elevated ducting layer. In (a): solid line is temperature, dotted line is dewpoint.

(iv) Surface duct

The fourth scenario given in Figure 9 represents a typical radiation-type inversion. The temperature increases with height while the dewpoint decreases rapidly with height. This type of situation results in a refractivity profile that decreases with height within the inversion layer and increases with height above.

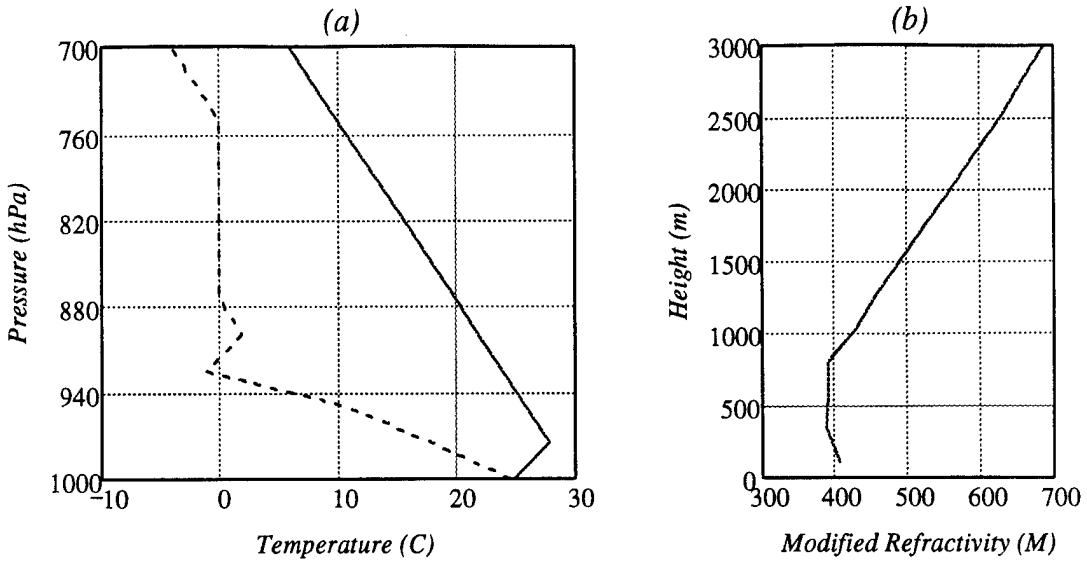

Figure 9. Radiosonde (a) and modified refractivity (b) profiles of an atmosphere with a surface or evaporation duct. In (a): solid line is temperature, dotted line is dewpoint.

2) RESOLUTION

The operational user of VTRPE will ultimately want to predict future conditions of electromagnetic propagation. The second aspect to this study is to use as inputs into the VTRPE model data from a current meteorological model that forecasts pressure, temperature, and humidity. To accurately portray the propagation, the forecast model must be of a sufficient resolution to capture the vertical and horizontal variability of the required parameters.

In 1993, an experiment in Variability Of Coastal Atmospheric Refractivity (VOCAR) was conducted off the coast of Southern California (Paulus, 1994). Data from Penn State's Mesoscale Modeling system (MM5) at 27 km horizontal resolution and 55 vertical layers was available for and used to generate the vertical refractivity profiles

that go into the VTRPE model[3]. Beginning with the maximum number of gridpoints and levels (representing the greatest resolution), VTRPE was run to generate a two-dimensional picture of the propagation conditions most-representative of the true atmosphere[4]. Subsequent simulations were run using fewer and fewer grid points, noting the changes in VTRPE results. These changes were compared to the original so that the effect of decreasing horizontal model resolution can be quantified.

Similar steps were performed by decreasing the number of vertical data levels in the model to simulate the effect of decreasing vertical model resolution.

b. Validation of model output

Future use of the VTRPE model depends on the ability to enhance the usefulness of radar operations. The VTRPE program must be able to correctly model the path of radar beam propagation through the atmosphere and provide new information to the radar user to enhance or correct operational analysis of radar signatures. There are many situations when the radar operator misinterprets returns that result from anomalous propagation. For example, a weather forecaster using a WSR-88D radar may identify "thunderstorms" only a few kilometers away when, in fact, they are returns of ground targets 100 or more kilometers away. These AP situations are most common when propagation ducts are present in the atmosphere. Given ducting situations as seen by the

[3] The data used was 24 Hour forecast data from the model run initialized at 12 UTC on August 29, 1993.

[4] This assumes that the MM5 model at 27 km resolution accurately portrays the coastal environment. The purpose of this study is not to determine how well MM5 models a marine boundary layer but to simply compare the effects of different resolution data.

radar, this study will determine if the VTRPE program correctly models the ducting or AP of electromagnetic radiation.

First, a "ducting" day was determined by the presence of anomalous propagation radar echoes as seen on the base reflectivity product from the WSR-88D radar located at Wilmington, OH. The upper-air data from the National Weather Service radiosonde launch site at Wilmington was used to generate a refractivity profile. Using VTRPE, the propagation path of the main lobe of the radar was calculated and analyzed to determine if the conditions predicted with VTRPE matched with what the radar operator sees.

c. Scope

Atmospheric effects on electromagnetic wave propagation are also frequency dependent. This study will be limited to examine the effects of propagation of an S-band radar (~ 3 GHz). S-band frequencies are commonly used for communications and weather radar. The WSR-88D radar, a meteorological radar widely used across the US and in several overseas locations, is an S-band radar and will be the focus of this study.

Although the model does account for terrain effects, this study will not investigate the sensitivity to variations of ground inputs. When applicable, terrain will be used, but the sensitivity to terrain will not be examined.

This study does not investigate how well a particular numerical model forecasts the meteorological parameters that go into calculating refractivity. Only the effect of model resolution is in question.

Chapter 4. Results and Discussion

a. Sensitivity to meteorological inputs

Four different atmospheric conditions were modeled: a standard atmosphere, a subrefractive atmosphere, an atmosphere with an elevated ducting layer, and an atmosphere with a surface evaporation duct. Figure 6 through Figure 9 of the previous chapter show the simulated radiosonde data and the corresponding refractivity profile for each of these meteorological environments.

For each of these atmospheric environments, five separate levels of maximum error (see Table 2, page 16) were introduced both independently and simultaneously into pressure (δP), temperature (δT), and relative humidity (δRH). This was done for thirty separate simulations for each variable and each environment. These collections of 30 soundings then represent sample populations where errors in pressure, temperature, and humidity are each taken independently and then collectively for each of the four environments.

1) ACCURACY

The sensitivity to measurement errors in pressure, temperature, and dewpoint (or humidity) showed a dependence on the type of environment surrounding the radar. The standard and subrefractive atmospheres produced comparable results. Also, though the evaporation and elevated ducts produced very different radar coverage diagrams, the error analysis produced similar results.

(i) Standard atmosphere

Figure 10 shows the radar coverage diagram of one-way propagation pathloss for the case of a standard atmosphere. The most noticeable feature is the pattern of peaks and nulls that result from areas of constructive and destructive interference from energy reflected off the earth's surface. Analogous to attenuation, higher values of pathloss indicate regions of lesser amounts of radar energy. Values greater than about 200 dB generally mean that a target cannot be detected by this radar, though this value may change depending on the specific target and radar.

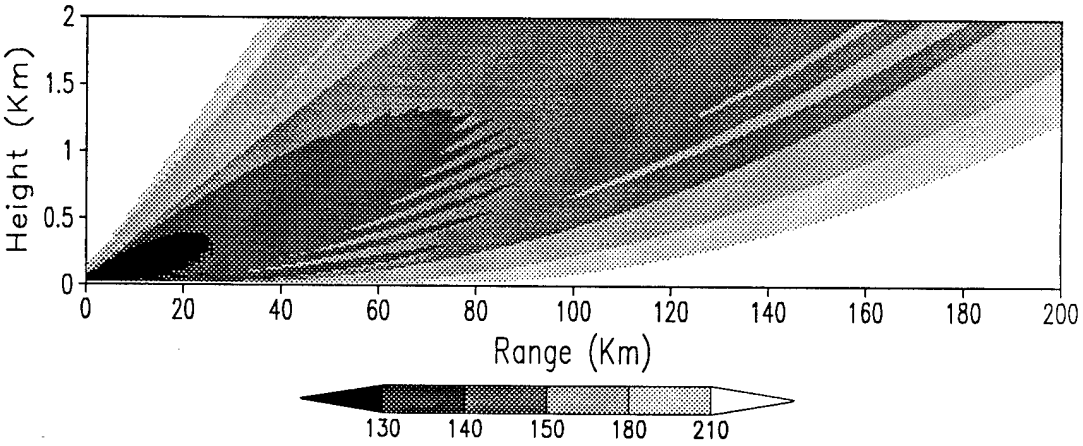

Figure 10. Radar coverage diagram of one way propagation pathloss (in dB) for a WSR-88D radar in a standard atmosphere.

Figure 11 shows the average RMS errors plus standard deviations of the 30 cases for a standard atmosphere. When all errors are included, the average RMSE is relatively constant at 1.8% with a standard deviation of 0.6%. Though this number seems very small, one must realize that it is only an error averaged over the entire range-height field of 2 km by 200 km. Figure 12 shows individual range-height diagrams of pathloss

uncertainty ($\Delta\beta$) averaged over the 30 simulations. Though the average over the entire region is only 1.8%, at long ranges and low altitudes the error can be as high as 15-20%.

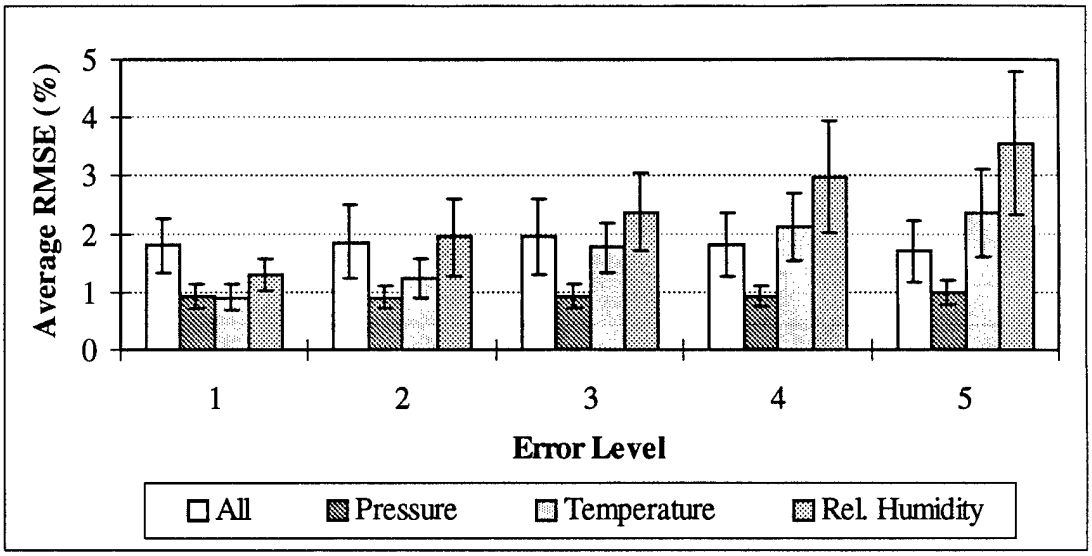

Figure 11. Average RMSE values and standard deviations of 30 simulations for a standard atmosphere. Columns represent the average RMSE (%) and error bars indicate one standard deviation around the average value.

These errors at low altitudes can be a critical distinction since a common military tactic for radar avoidance is to "fly low". For example, suppose a particular military aircraft could not be "seen" by this S-band radar at values of propagation pathloss above 210 dB. One method to avoid detection by this radar in a standard atmosphere would be to fly lower than 1 km altitude within 200 km range of the radar (Figure 10). If however, the pathloss error in this region is 10 percent (± 21 dB or greater) the aircraft may become detectable simply due to measurement errors of pressure, temperature, and humidity.

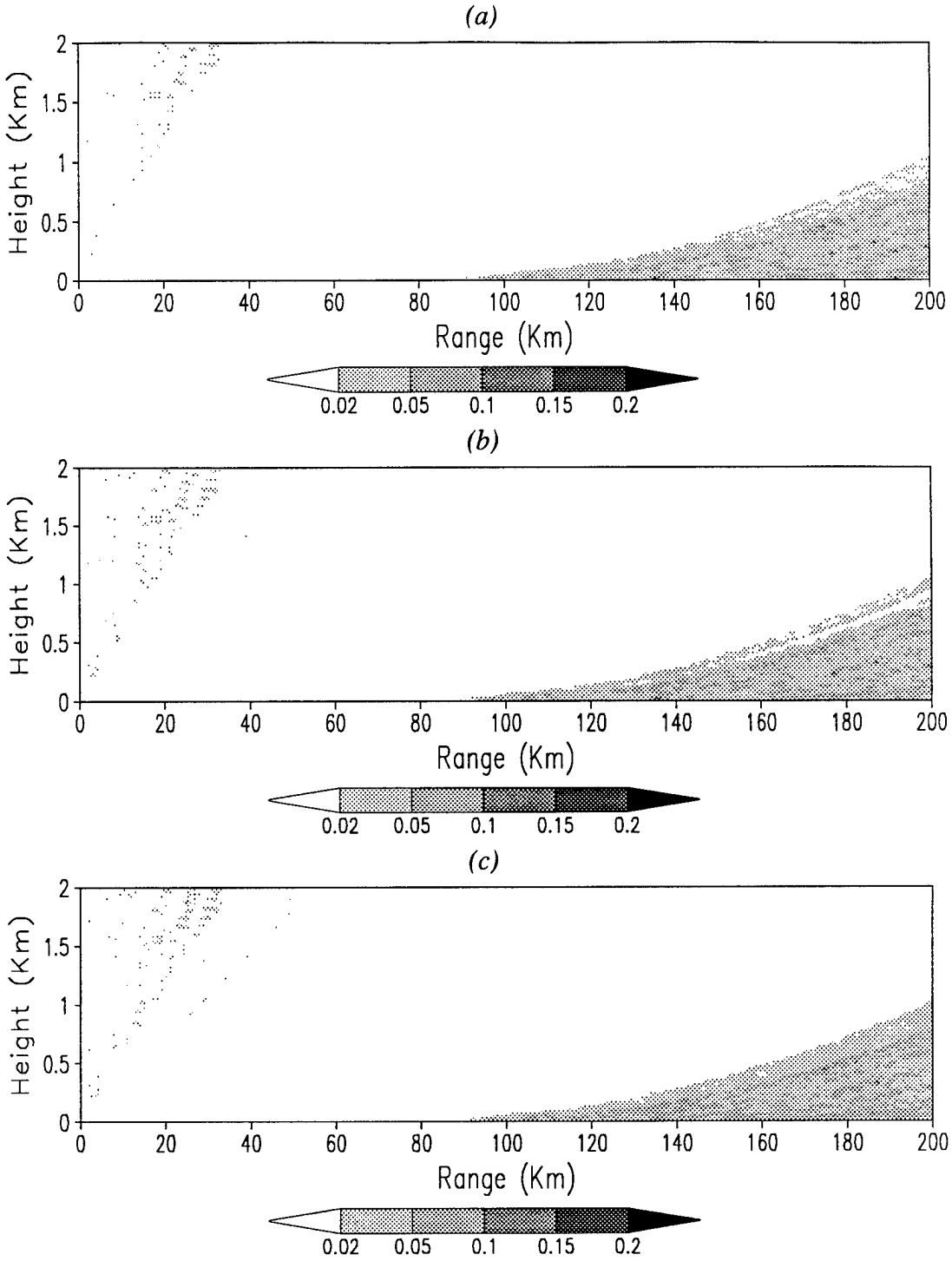

Figure 12. Range-height diagrams of average uncertainty, $\Delta\beta$ (%), of 30 simulations in pathloss for standard atmosphere where all variables are allowed to have errors. (a) shows error level one, (b) error level two, (c) error level three. On next page: (d) error level four, and (e) error level five.

(d)

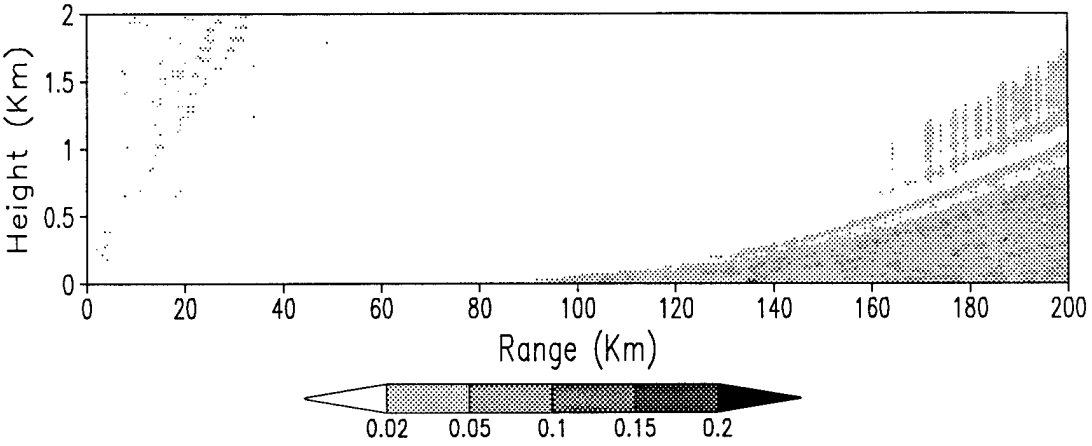
Height (Km)
2
1.5
1
0.5
0
0
20
40
60
80
100
120
140
160
180
200
Range (Km)
0.02
0.05
0.1
0.15
0.2

(e)

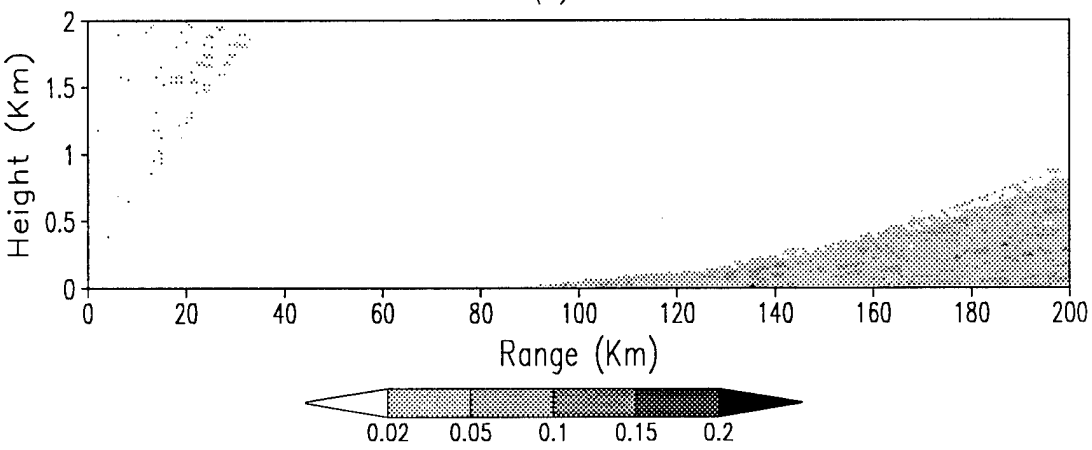
Height (Km)
2
1.5
1
0.5
0
0
20
40
60
80
100
120
140
160
180
200
Range (Km)
0.02
0.05
0.1
0.15
0.2

When the errors in atmospheric parameters are taken independently, considerably different results occur. Errors in relative humidity consistently result in larger values of RMSE than either pressure or temperature. This result is consistent with the discussion about errors in calculating N in Chapter 2. In Table 2 the constants for humidity (c_3) were consistently greater than the others. Like refractivity, propagation pathloss is most sensitive to measurements of humidity in a standard atmosphere.

When the maximum error in measuring humidity (δRH) is ±1% the average RMSE for the VTRPE range-height output is only 1.3% but increases to 3.5% when δRH is ±5%. Again, this represents only an average over the entire range-height field. Figure 13 shows these range-height diagrams of average uncertainty. When δRH is ±1%, there is a small area of 2-5% uncertainty beyond 100 km range and below 0.5 km altitude. However, when δRH increases to 3%, this area expands significantly and increases to a maximum uncertainty of 5-10%. At δRH= ±5% nearly half of the coverage beyond 100 km range contains errors greater than 5%.

The RMSE due to errors in pressure (δP) is nearly constant at 0.9% for all levels of maximum error, the smallest of the three parameters. Errors in temperature (δT) produced the second highest RMSE values, from 0.8% increasing to 2.4%. Range-height diagrams of average uncertainty (not shown) reveal similar error results as those shown in Figure 12 and Figure 13, but the areal coverage and maximum error are proportional to the average RMSE values shown in Figure 11.

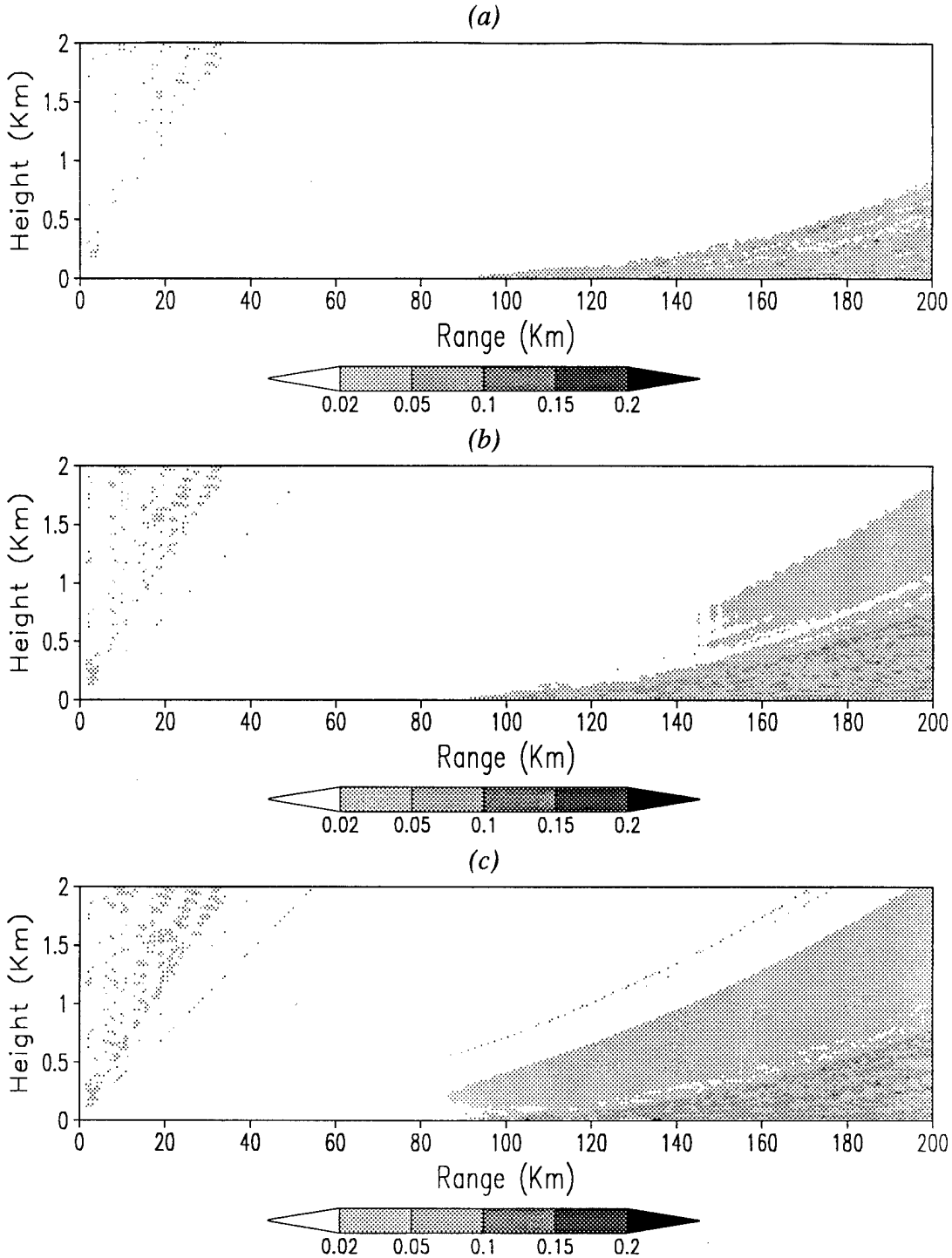

Figure 13. Range-height diagrams of average uncertainty, $\Delta\beta$ (%), of 30 simulations in pathloss for a standard atmosphere with errors in measuring relative humidity. (a) δRH= $\pm$1%, (b) δRH= $\pm$2%, (c) δRH= $\pm$3%. On next page: (d) δRH= $\pm$4%, (e) δRH= $\pm$5%.

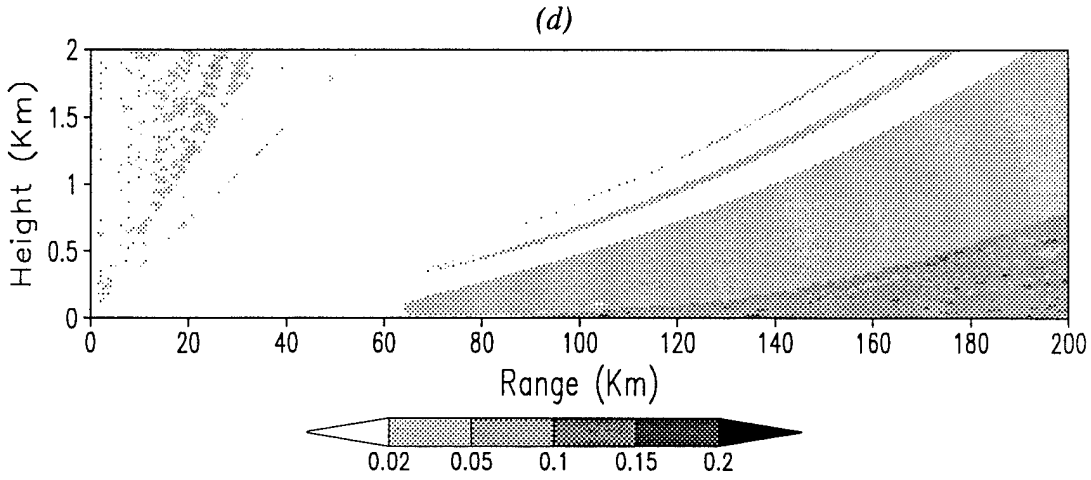
(d)
Height (Km)
2
1.5
1
0.5
0
0
20
40
60
80
100
120
140
160
180
200
Range (Km)
0.02
0.05
0.1
0.15
0.2

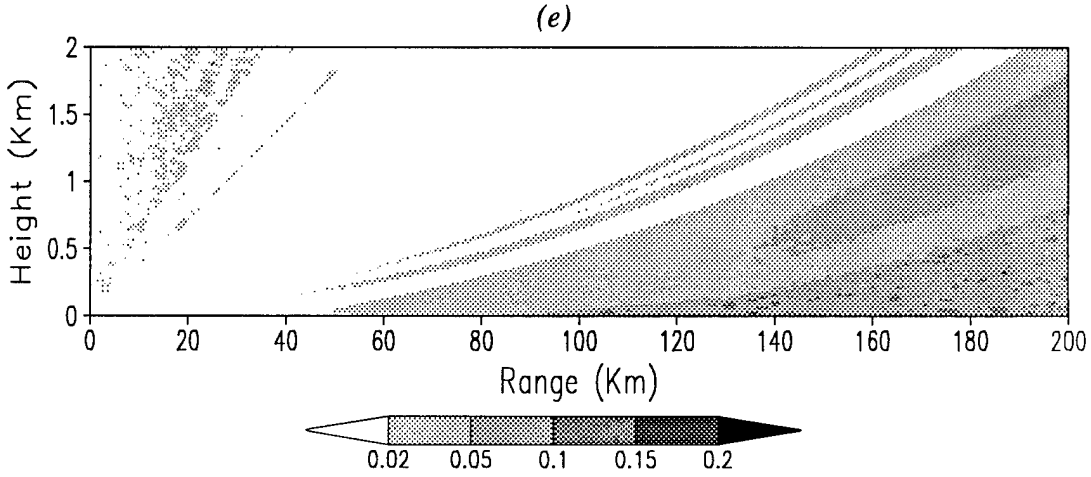
(e)
Height (Km)
2
1.5
1
0.5
0
0
20
40
60
80
100
120
140
160
180
200
Range (Km)
0.02
0.05
0.1
0.15
0.2

Overall, the uncertainty in calculating propagation pathloss tends to increase as the errors increase in pressure, temperature, and humidity independently. However, when the sum of all errors is included in the calculation, this tendency is smoothed or even leveled to become nearly constant regardless of the error level. One suggestion is that these errors tend to cancel each other out. Referring back to Table 2, the constants referring to temperature errors has a negative contribution to the RMS errors while the constants for pressure and vapor pressure contribute positively to RMS errors. It's been said that "two wrongs do not make a right" however, in this case it appears that they do. Also, since the random errors are allowed to be positive or negative, a positive error in pressure may be canceled by a negative error in vapor pressure so that the overall error in refractivity is smaller than the two individually.

(ii) Subrefractive atmosphere

Figure 14a shows the radar coverage diagram of propagation pathloss in a subrefractive atmosphere. This diagram appears nearly identical to that for the standard atmosphere, however, the differences become apparent in Figure 14b where the difference field is plotted. Though the greater part of the coverage has less than 5 dB difference, at lower elevations beyond 60 km the pathloss is up to 45 dB greater for the subrefractive environment.

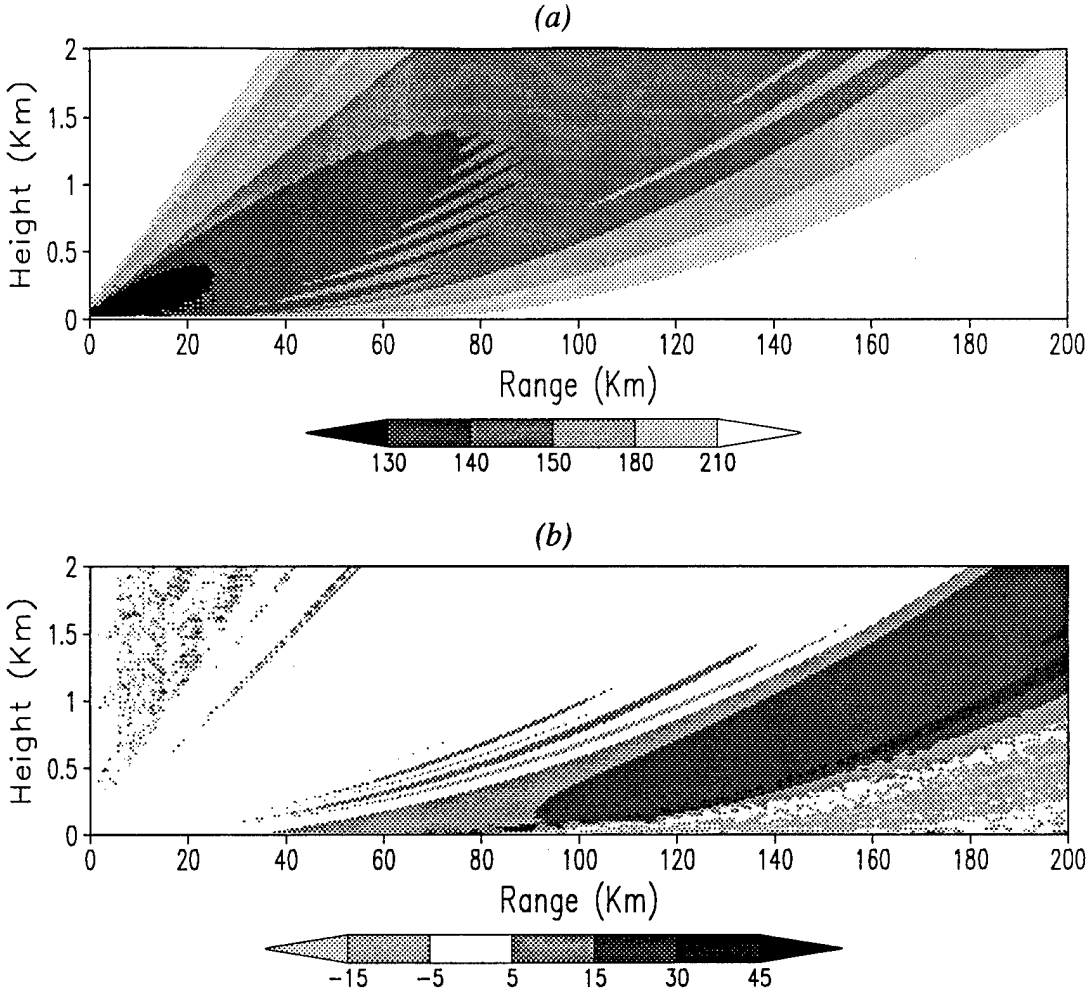

Figure 14. Radar coverage diagram (a) of propagation pathloss (dB) for a subrefractive atmosphere, and relative difference (dB) from a standard atmosphere (b). Positive values show where pathloss is greater than for the standard atmosphere.

Figure 15 summarizes the average RMS errors and standard deviations of 30 simulations in a subrefractive atmosphere. It shows an even stronger contrast between the individual parameters than in a standard atmosphere. When errors are introduced into all variables, RMSE is nearly constant at 1.8% with a 0.5% standard deviation. However, when only errors in measuring humidity are allowed, the RMSE values are distinctly greater than for the other parameters and more than double as δRH increases from 1% to

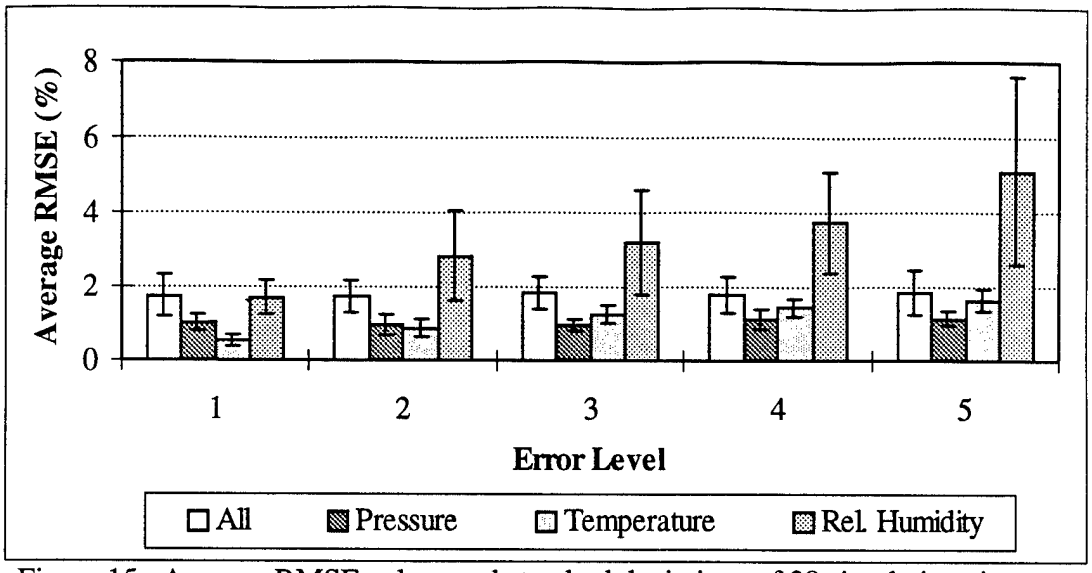

Figure 15. Average RMSE values and standard deviations of 30 simulations in a subrefractive atmosphere. Columns represent the average RMSE (%) and error bars indicate one standard deviation around the average.

5% error. The standard deviation of RMSE values also rises dramatically from 0.45% at $\delta RH = \pm 1\%$ to 2.5% at $\delta RH = \pm 5\%$. When only errors in pressure are allowed, the average RMSE values are nearly constant at 1.0%. When only errors in temperature are allowed, the average RMSE values rise gradually from 0.5% at $\delta T = \pm 0.2$ C to 1.6% at $\delta T = \pm 2.0$ C.

Like the standard atmosphere case, the calculation of propagation pathloss in a subrefractive atmosphere is most sensitive to moisture measurements when the errors are considered independently. However, this sensitivity is nearly eliminated when all measurement errors are included in the refractivity calculations. The overall pathloss uncertainty is less than 2%. In the region beyond 100 km in range the uncertainty can be as high as 2-5% (Figure 16).

(iii) Elevated ducting layer

Figure 17 shows the radar coverage diagram for an elevated ducting layer which again, looks in many ways very similar to the diagram for standard atmosphere. Close examination of Figure 10 and Figure 17 reveal two subtle yet important differences. One difference is in the 180-210 dB pathloss contour at long ranges beneath the main beam of the radar. In a standard atmosphere (Figure 10) this region is characterized by pathloss values greater than 210 dB. In an atmosphere with an elevated duct, clearly energy is being refracted into this region (and reflected off the earth's surface) so that pathloss is decreased to 180-210 dB. A second difference exists in the 180 dB pathloss contour. Compared with the standard atmosphere, the 180 dB pathloss contour suggests that the main energy lobe of the radar is subrefracted.

When the difference between this case and the standard atmosphere case is plotted, we find that this example is remarkably similar to the subrefractive case. An analysis of the refractivity profile shows a very strong subrefractive layer near the earth's surface beneath the elevated duct. Though some energy is being ducted by the elevated duct, it appears that the environment immediately surrounding the radar has more bearing on the main path of radar energy than the elevated duct itself.

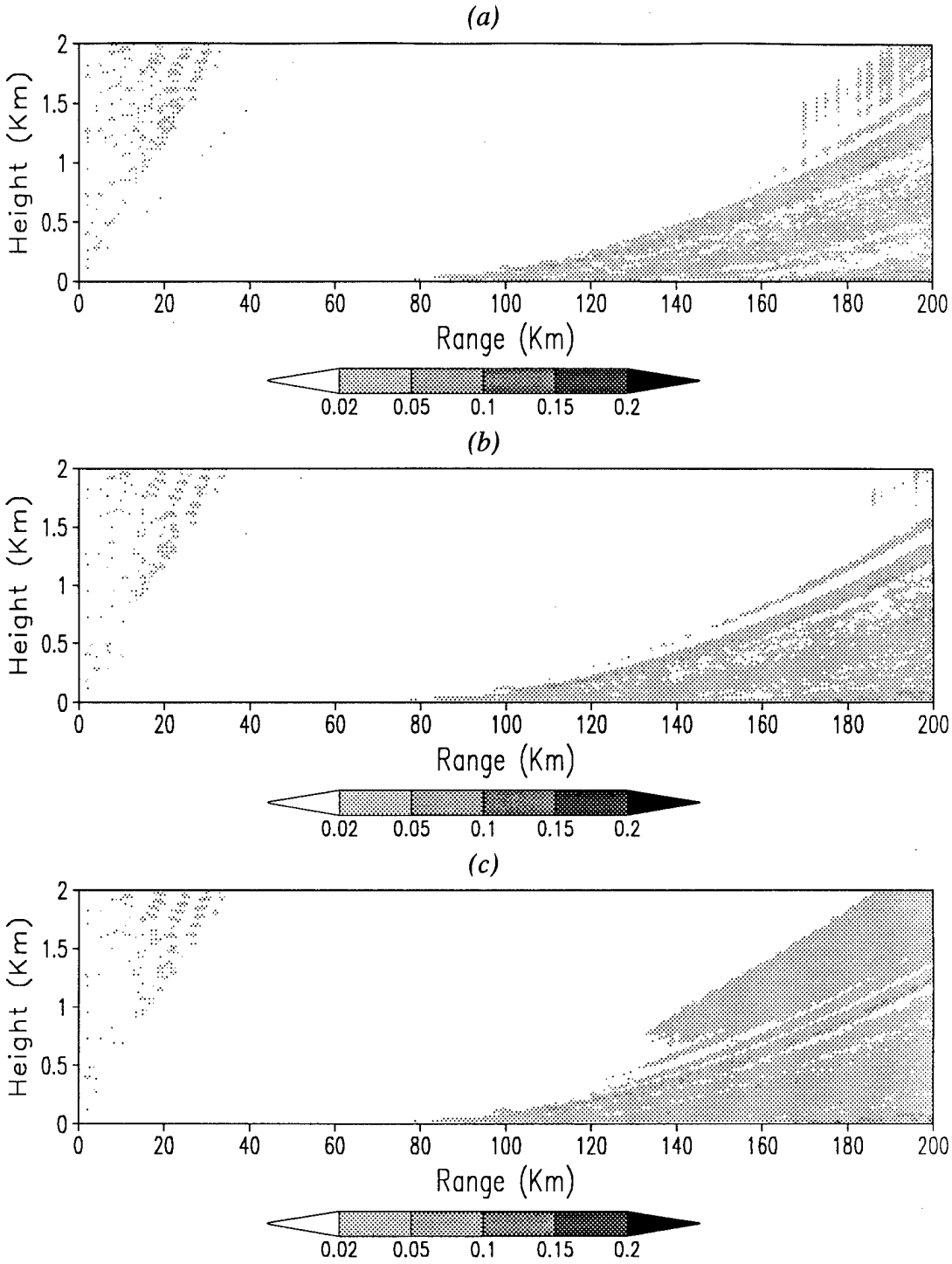

Figure 16. Range-height diagrams of average uncertainty, $\Delta\beta$ (%), of 30 simulations in pathloss for subrefractive atmosphere where all variables are allowed to have errors. (a) shows error level one, (b) error level two, (c) error level three. On next page: (d) error level four, and (e) error level five.

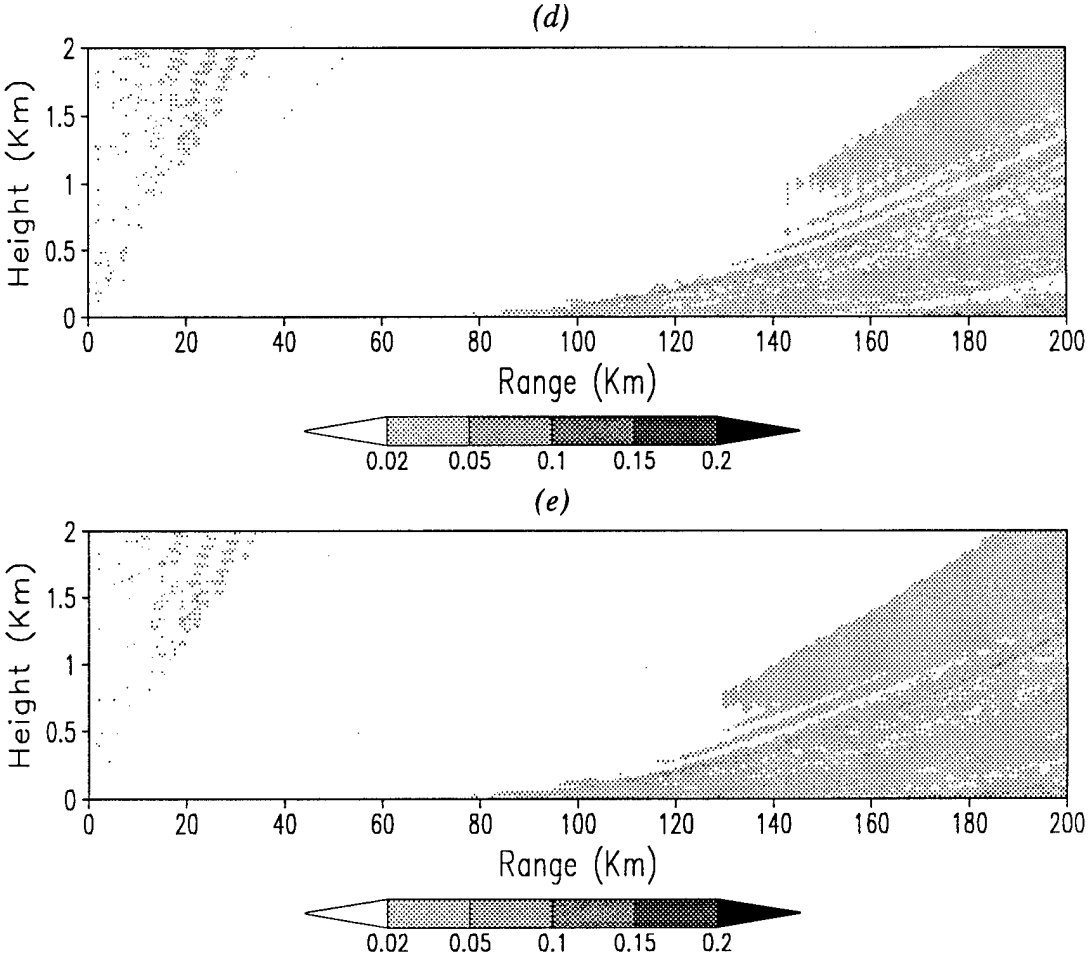
(d)
Height (Km)
2
1.5
1
0.5
0
0
20
40
60
80
100
120
140
160
180
200
Range (Km)
0.02
0.05
0.1
0.15
0.2
(e)
Height (Km)
2
1.5
1
0.5
0
0
20
40
60
80
100
120
140
160
180
200
Range (Km)
0.02
0.05
0.1
0.15
0.2

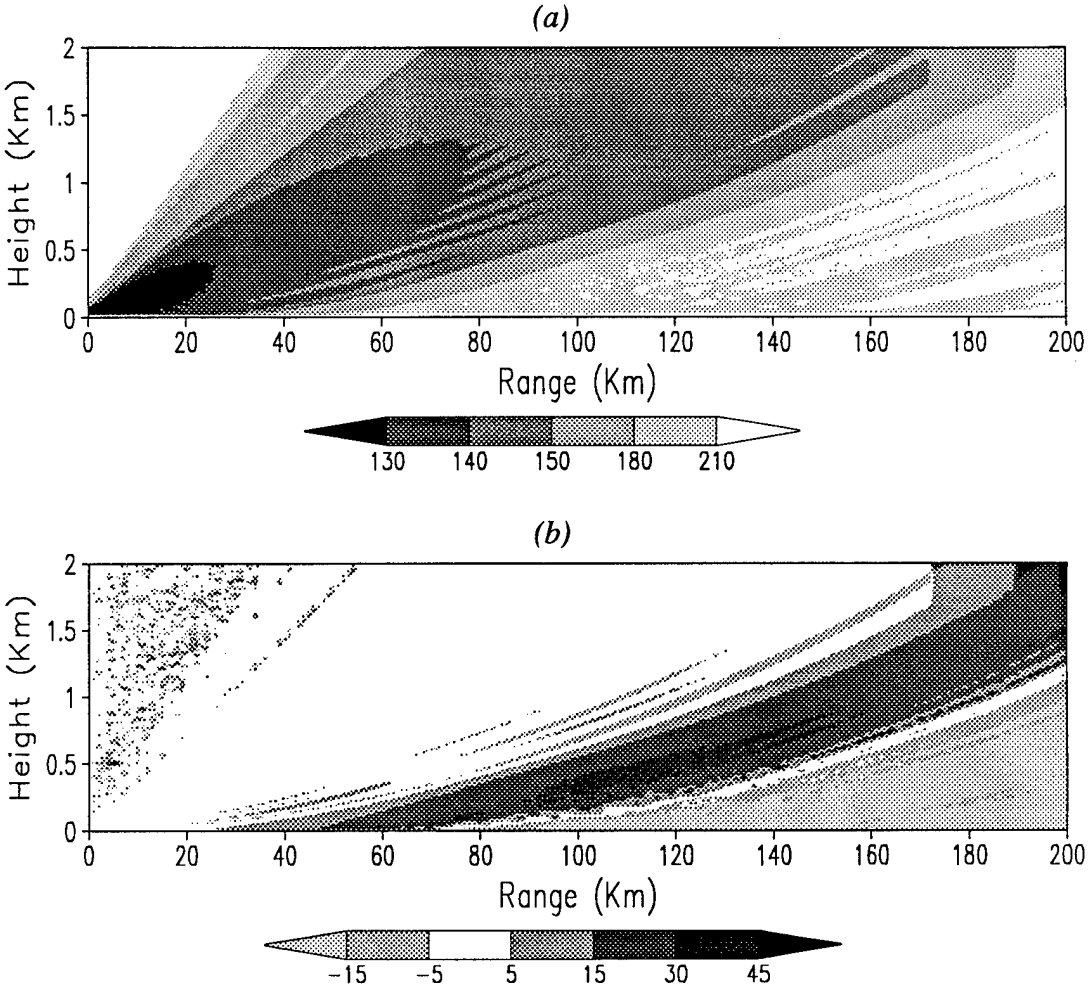

Figure 17. Radar coverage diagram (a) of propagation pathloss (dB) for an atmosphere with an elevated ducting layer, and relative difference (dB) from a standard atmosphere (b). Positive values show where pathloss is greater than for the standard atmosphere.

When the error sensitivity is examined, the elevated ducting case offers several differences from the previous two cases. Figure 18 summarizes the average RMSE values and standard deviations of 30 simulations in this environment. When pressure, temperature, and humidity measurements are allowed to vary, the average RMSE hovers around 2.2% compared to 1.8% in the standard and subrefractive atmospheres.

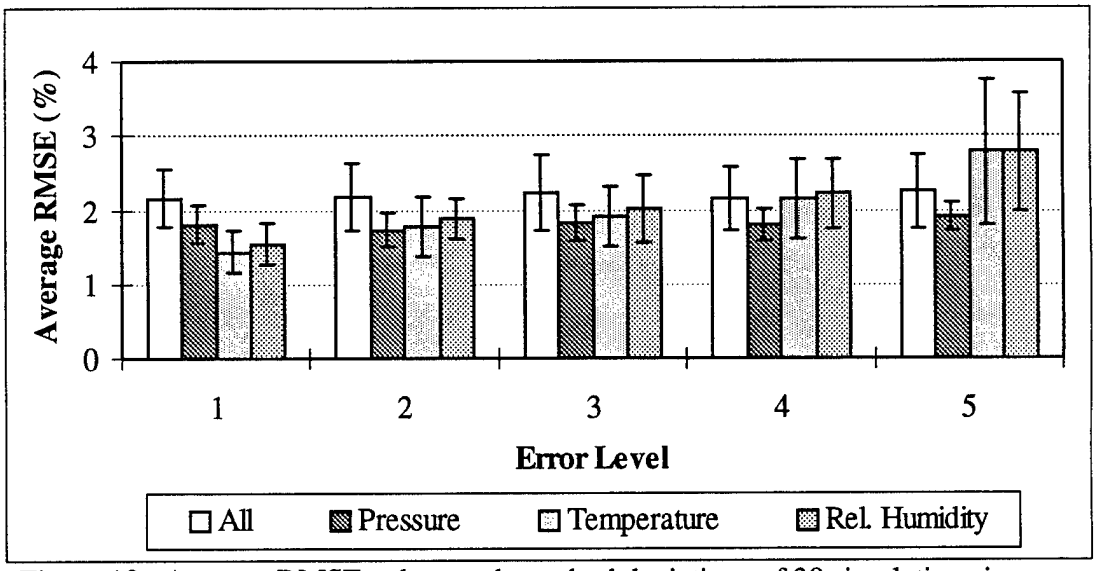

Figure 18. Average RMSE values and standard deviations of 30 simulations in an atmosphere with an elevated ducting layer. Columns represent the average RMSE (%) and error bars indicate one standard deviation around the average value.

When considered independently, no single parameter stands out as causing substantially greater RMSE than any other. Like the previous two cases, errors due to measurement of pressure remain essentially constant at 1.8% RMSE regardless of the level of measurement error. RMSE due to temperature and humidity measurement errors show a tendency to increase from around 1.5% RMSE at error level 1 to near 3% RMSE at error level 5. One other feature is that standard deviations are generally lower overall than

either in a standard or subrefractive atmosphere. This suggests a smaller variability in propagation calculations.

(iv) Surface evaporation duct

The case for a surface ducting atmosphere produced the greatest deviation from standard for the radar coverage diagram, but average errors were generally the lowest of the four cases. Figure 19a shows how the radar energy is trapped between the earth's surface and the top of the propagation duct at 337 meters. In Figure 19b, this represents a 5 dB to over 100 dB decrease (relative to a standard atmosphere) of pathloss (thus increase in radar energy) in the lower elevations at ranges beyond 40 km.

Figure 20 summarizes the average RMSE and standard deviations when errors are introduced into the sounding data. Similar to the elevated ducting case above, no single meteorological parameter stands out as causing larger values of RMSE. When pressure, temperature, and humidity are allowed to vary, the average RMSE is 1.8%, compared to 2.2% in the previous case. When errors are introduced independently, all show an equal tendency to increase from around 1.3% at error level one to just over 2% at error level five. This is about 1% lower than in the elevated duct case.

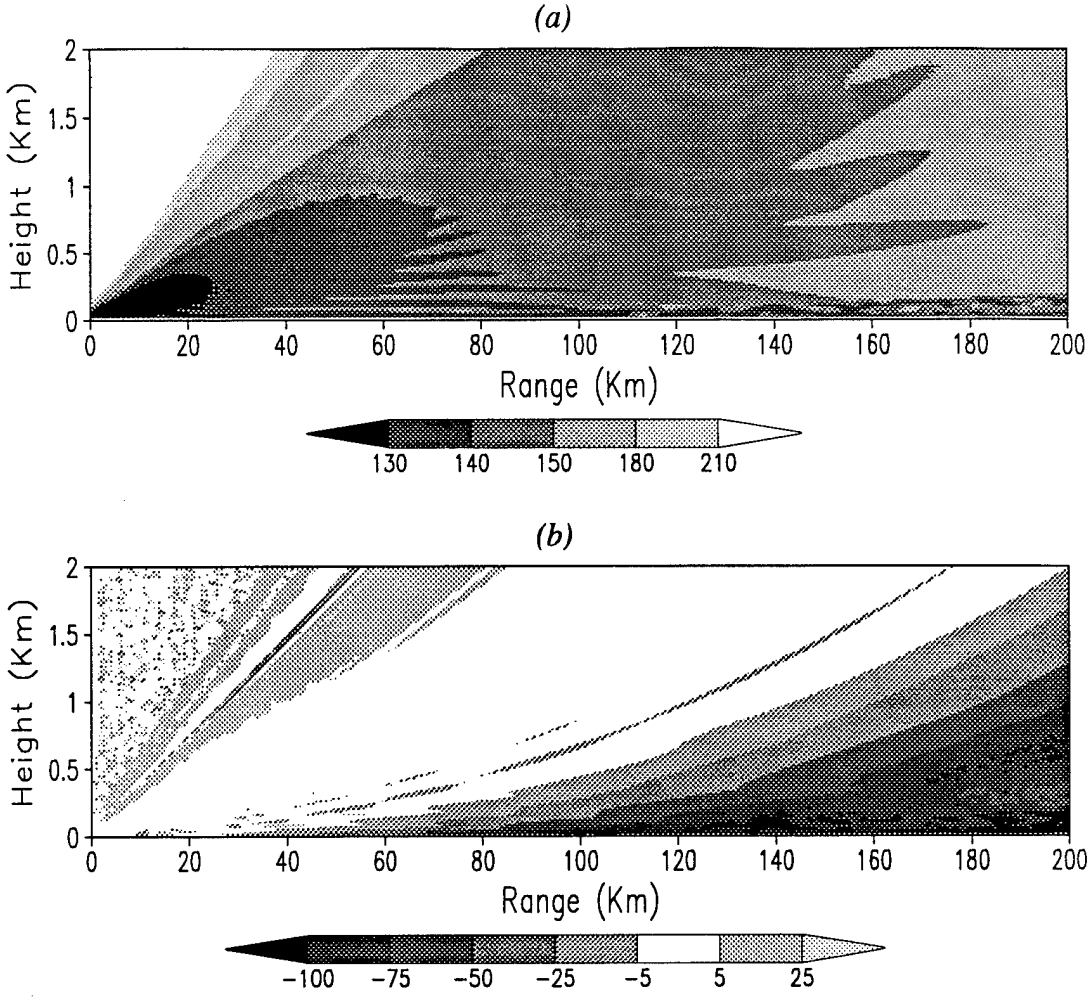

Figure 19. Radar coverage diagram (a) of propagation pathloss (dB) for an atmosphere with a surface evaporation duct, and the relative difference (dB) from standard atmosphere (b). Positive values show where pathloss is greater than for the standard atmosphere.

The most noticeable difference is that sensitivity to pressure measurement is considerably more significant (1.3 to 2% average RMSE) than the previous case. One hypothesis is that pressure is significant in the calculation of height through the hypsometric equation (see Appendix B). When a surface evaporation duct is present, height calculations become much more critical since the vertical gradient of refractivity is

crucial in the calculation of energy propagation. This dependence on pressure measurements does not exist in any of the other environments.

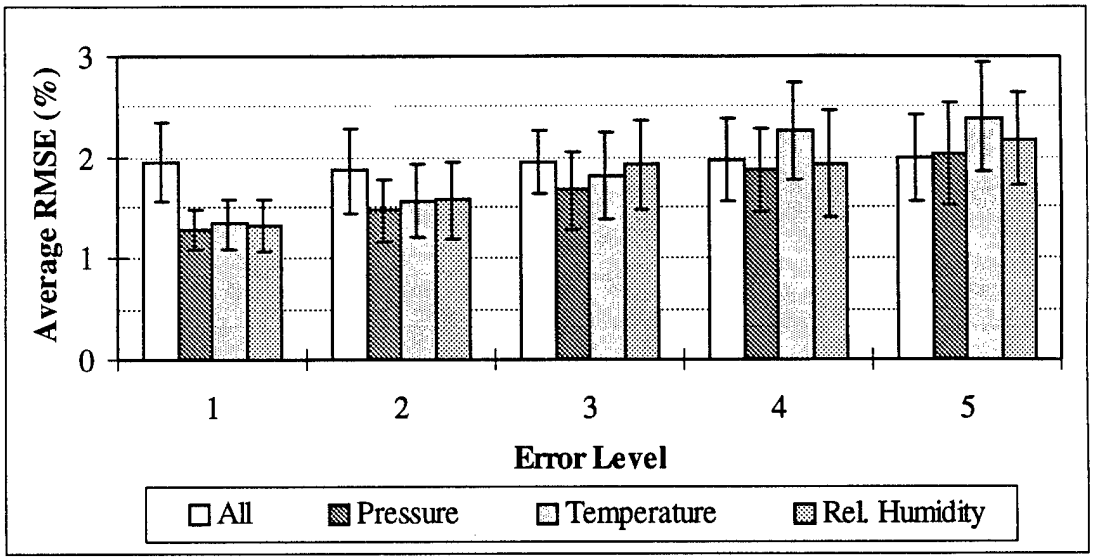

Figure 20. Average RMSE values and standard deviations of 30 simulations in an atmosphere with surface evaporation duct. Columns represent the average RMSE (%) and error bars indicate one standard deviation around the average value.

Another difference between the surface duct and the elevated duct is in the standard deviations. Overall, the deviations from the surface duct example tend to be the smallest of the four environments. This suggests that pathloss calculations have much less variability in an evaporation duct environment than in an elevated duct environment.

This is more evident when comparing the range-height diagrams of pathloss uncertainty. Figure 21 shows range-height diagrams of pathloss uncertainty averaged over 30 simulations where level two errors are introduced into pressure, temperature, and humidity. With the elevated duct, a large area of error greater than 2% exists from the surface at 60 km to over 2 km in altitude at 200 km range. This diagram is very similar to one for a subrefractive atmosphere with no duct. The reason for this similarity appears to

be the subrefractive layer beneath the elevated duct layer. In both the subrefractive and elevated duct environments, pathloss uncertainty of 2 to 5% extends to well over 2 km altitude at 200 km range. This again suggests that the propagation of radio waves is most sensitive to the low-level environment immediately surrounding the radar. In the surface duct environment, similar to the energy itself, the errors in propagation measurement are confined to a region from 30 to 200 km in range up to only 500 m in altitude.

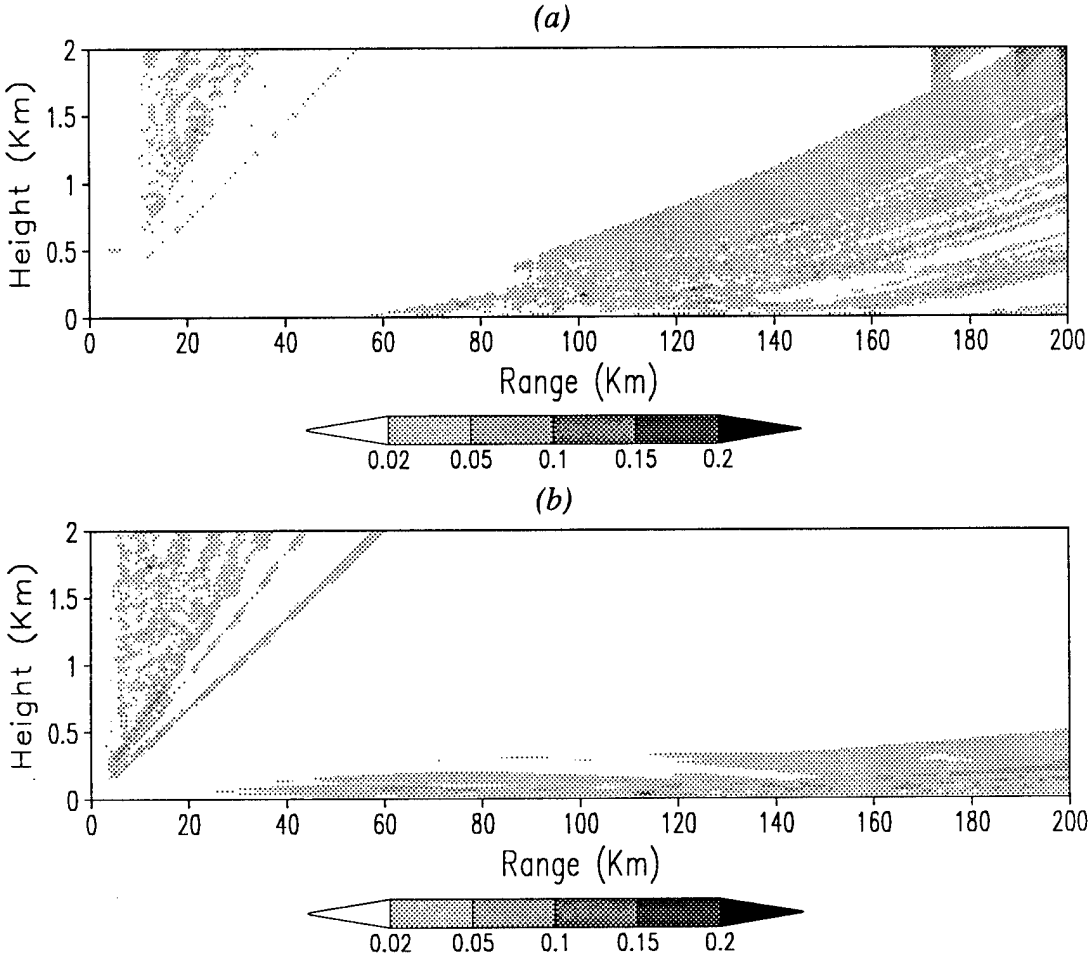

Figure 21. Range-height diagrams of pathloss uncertainty (in percent) averaged over 30 simulations where level two errors are introduced into pressure, temperature, and humidity. (a) represents an atmosphere with an elevated duct and (b) an atmosphere with a surface evaporation duct.

2) RESOLUTION

The sensitivity of VTRPE pathloss output to varying data resolution was tested using Penn State's MM5 mesoscale model output for the Variability of Coastal Atmospheric Refractivity (VOCAR) experiment conducted off the Southern California coast in 1993 (Paulus, 1994). A 216 km cross-section of pressure, temperature, and humidity data was chosen to represent a typical transition from a marine to a continental boundary layer (Figure 22). The refractivity profiles generated from the MM5 model data are shown in Figure 23. Although these profiles do exhibit some horizontal variations,

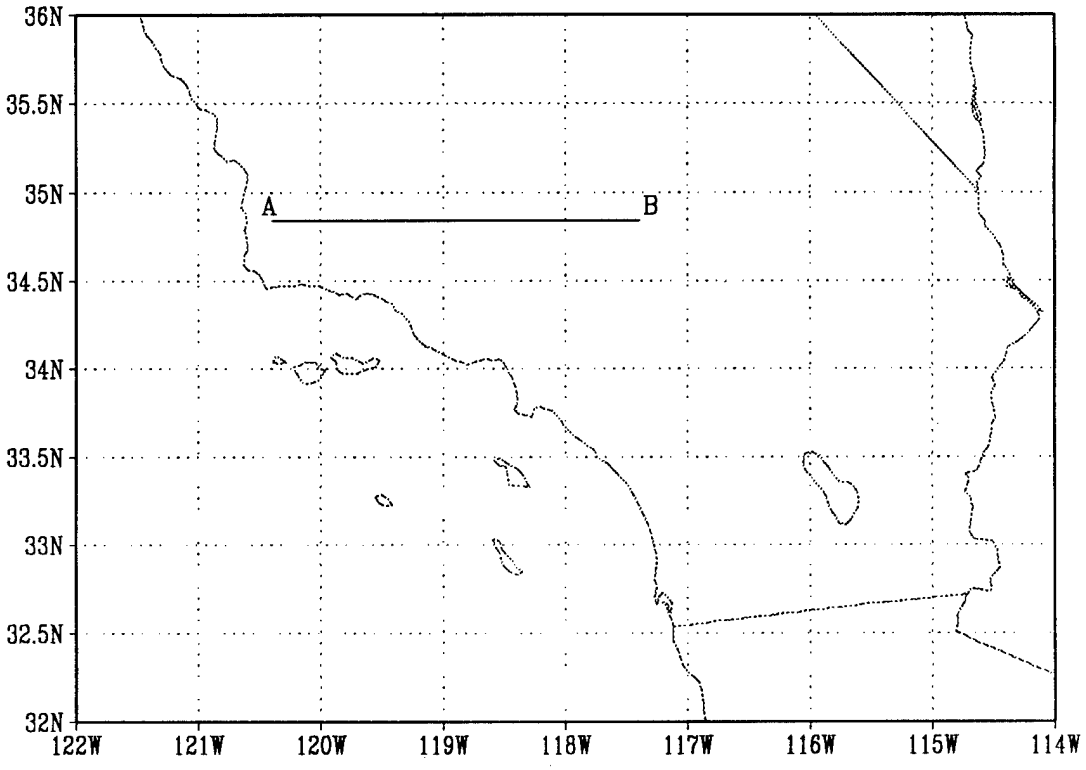

Figure 22. Map of the VOCAR experiment area. Solid line AB at 34.8 N represents the location of the cross-section taken for refractivity profiles.

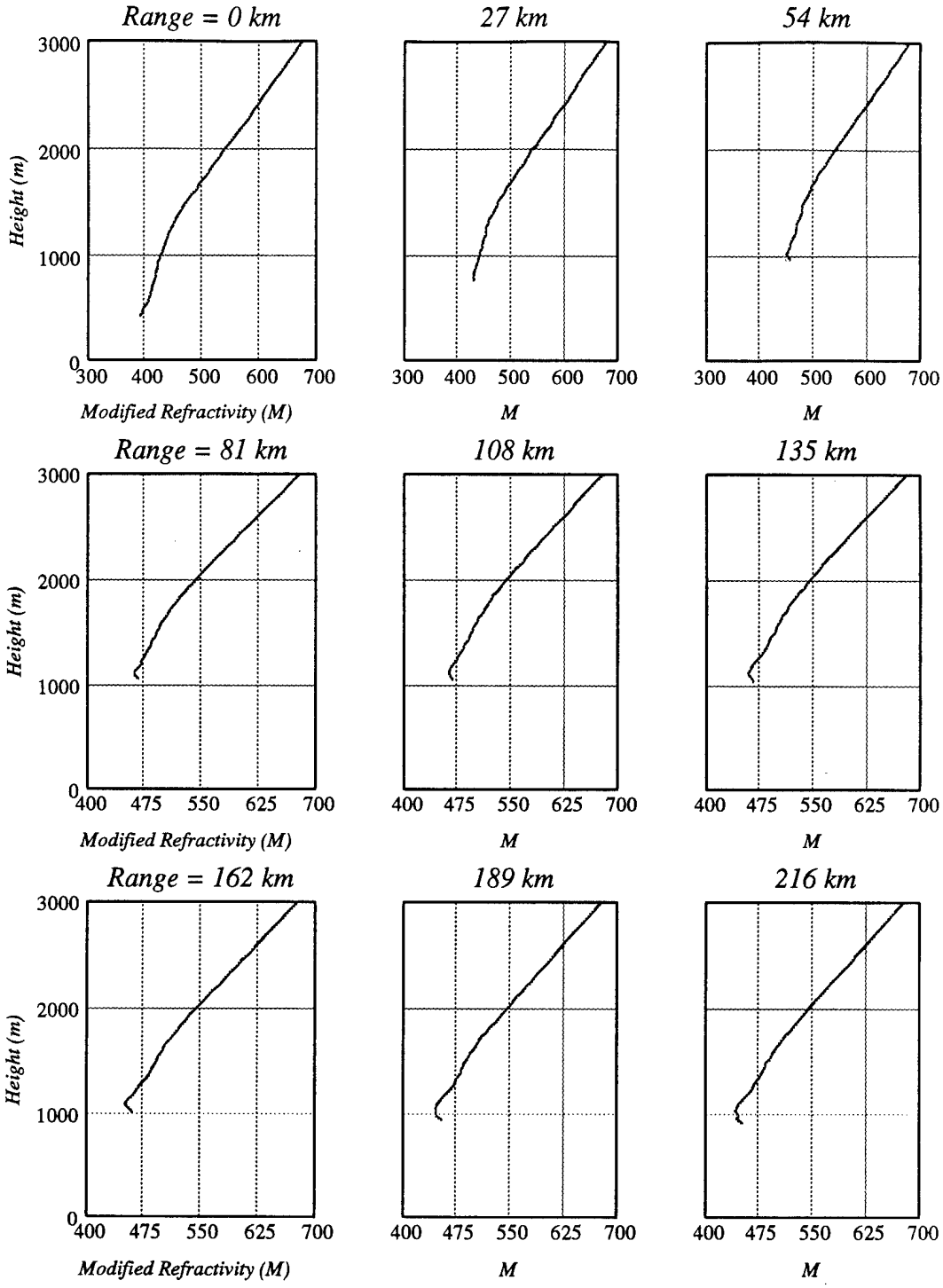

Figure 23. Refractivity profiles along the cross-section identified in Figure 22. Ranges indicate the distance from point A.

these changes are not great. At 0 and 27 km, even in the presence of a strong subsidence inversion over a moist marine layer, there are no propagation ducts. The layer from the surface to about 1200 meters is superrefractive and nearly standard above 1200 m. At 54 km and beyond, each of the profiles have a surface evaporation duct. This is likely a result of radiational cooling of the earth's surface in the higher terrain.

When the highest resolution data is used (all nine profiles at 27 km resolution) the radar coverage diagram generated by VTRPE represents the best possible calculation of propagation conditions with the data available.[5] Figure 24a shows the radar coverage diagram of propagation pathloss along the line AB for a radar located at point A in Figure 22. The most notable feature is the effect of terrain on radar coverage. Targets located beyond 120 km in the shadow of the mountains are virtually undetectable due to the pathloss values of 220 dB or greater. However, in the 60-100 km range between the mountain peaks the pathloss values are only between 160 and 190 dB. It is possible that targets here can be detected, even though they are not within line-of-sight of the radar.

As data resolution decreases, one would expect the calculated pathloss to differ significantly as meteorological information is lost. Figure 24b and Figure 24c shows the difference result of reducing the horizontal resolution to 54 km and 81 km respectively. Overall, there is very little change when the horizontal data resolution is reduced. The greatest portion of both 54 km and 81 km cases has less than a ±2 % change in pathloss values from the 27 km case. The two regions of greatest variability lie just above the mainlobe at 40 to 80 km and in the shadow of the mountain beyond 130 km. In both areas

[5] Actual measurements of radar data was not available during this experiment so it was assumed that this calculation represented ground truth. All other variations were compared to this result.

the difference from the 27 km data is about ±2-5 % (5 - 10 dB) with widely scattered areas of up to ±5-10 % (15 dB) difference.

Similarly, the vertical resolution was reduced from 55 to 28 and 18 levels. Radar coverage diagrams for these reduced vertical resolutions were compared with the results from the original 55 layer model. Figure 25a shows the result of using only half of the available data levels. Overall, there is less than a ±2% difference through most of the region. In the lee of the mountain peaks the error is as large as ±5% with widely scattered regions of 5-10% error. The area of greatest differences is just above the mainlobe of the radar between 20 and 90 km. In this region, reducing the vertical resolution can result in an error of just over ±20%. When the resolution is decreased to only 18 data levels (Figure 25b), the radar coverage diagrams show no noticeable increase in these differences. At the highest resolution of 55 data levels, the vertical spacing is about 50 meters. When the number of levels is decreased to 28 and 18, the vertical spacing is increased to about 100 and 150 meters respectively. Apparently, most of the information loss occurs at the initial 50% reduction of resolution. No additional significant information is lost when the vertical levels decrease from 28 to 18.

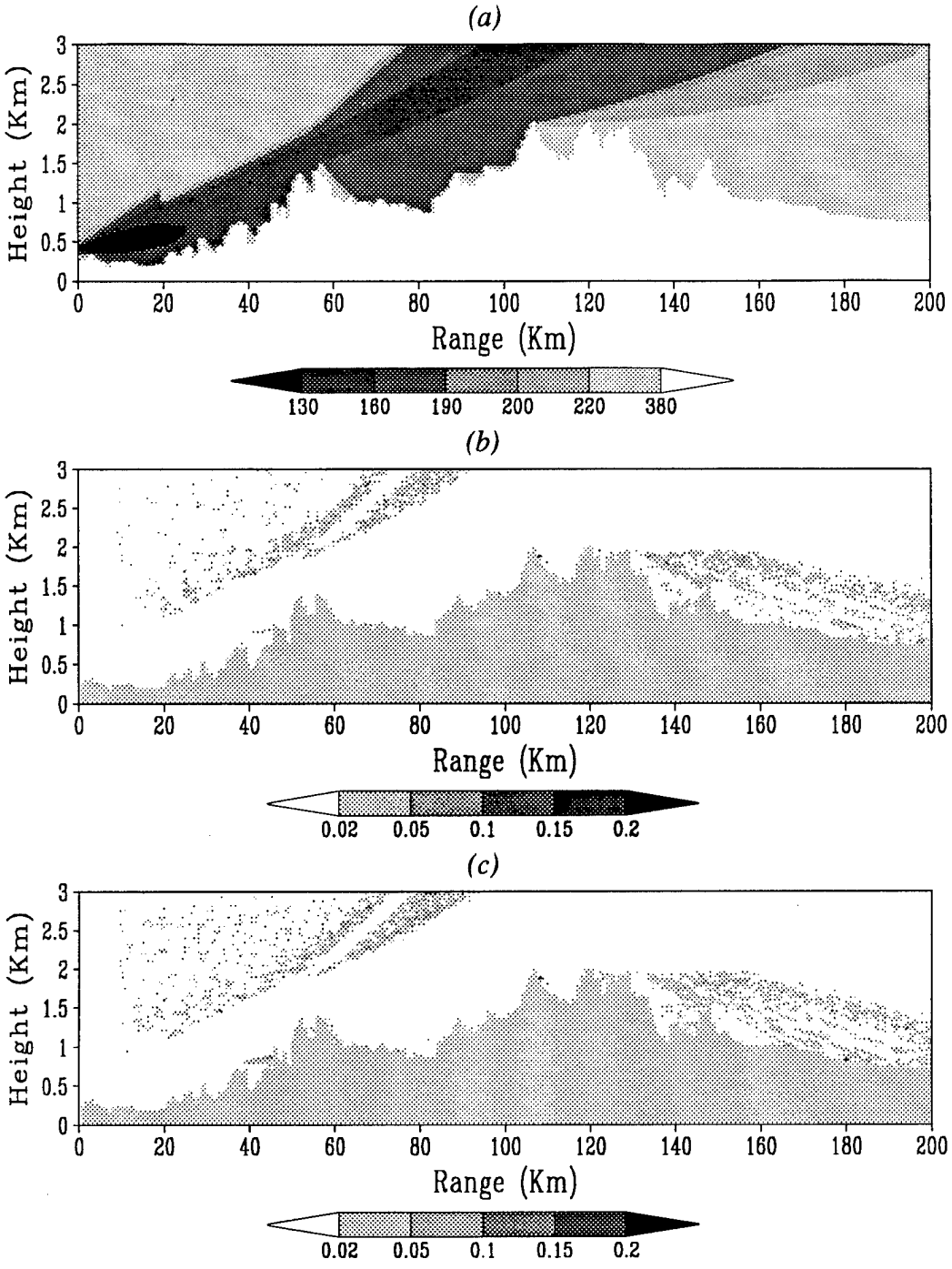

Figure 24. In (a) Radar coverage diagram of propagation pathloss (dB) along line AB in Figure 22. In (b) the absolute difference (%) between coverage diagrams at 54 km and 27 km resolution. In (c) the difference (%) between coverage diagrams at 81 km and 27 km resolution. Shaded region in (b) and (c) indicates terrain.

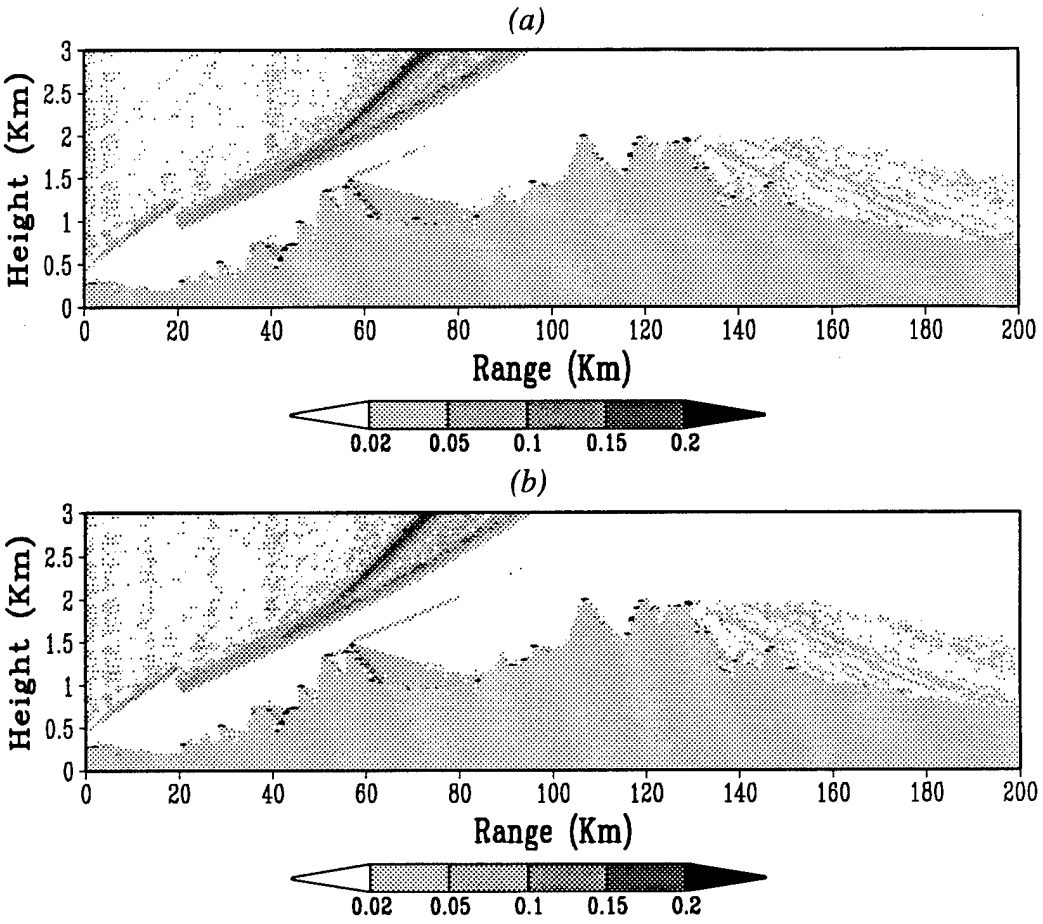

Figure 25. Absolute difference (%) diagrams resulting from the reduction of vertical levels in the MM5 data at 27 km horizontal resolution. In (a) the absolute difference (%) between coverage diagrams at 28 and 55 levels. In (b) the difference (%) between coverage diagrams 18 and 55 levels. Unshaded region indicates terrain.

A possible explanation for this weak dependence on resolution is that the initial data itself does not have any strong horizontal or vertical variations in gradients of refractivity. Though horizontal and vertical variations do exist, Figure 23 does indicate that these variations are not very strong. Each of the vertical profiles of refractivity are very similar to each other. Therefore, even if several profiles are removed, the calculation of propagation pathloss will not be significantly different. In the vertical, the gradient of refractivity is relatively constant. The only profiles that have significant changes in the vertical gradient are those beyond 54 km. These profiles have surface evaporation layers of negative M gradients. However, these gradient changes occur only in the atmosphere immediately next to the earth's surface. At these distances from the radar, the effect on propagation is negligible.

Another possible explanation deals with the problem of terrain. When using VTRPE to model propagation, very-high resolution terrain data was available from the Department of Defense Digital Terrain Elevation Database (DTED) on CD-ROM. However, the MM5 model uses a much coarser resolution terrain. Figure 26 compares the DTED terrain data and the MM5 model terrain data along the same cross-section AB in Figure 22. The MM5 terrain is much smoother and almost unrepresentative of the actual terrain used in the VTRPE model. Close comparison of Figure 26a and Figure 26b reveals that in several locations the model terrain lies below the actual surface because of this smoothing. This results in a loss of data in the lowest elevations of the model data. If the greatest variations in refractivity gradient occur near the model surface, this may result in serious VTRPE calculation errors.

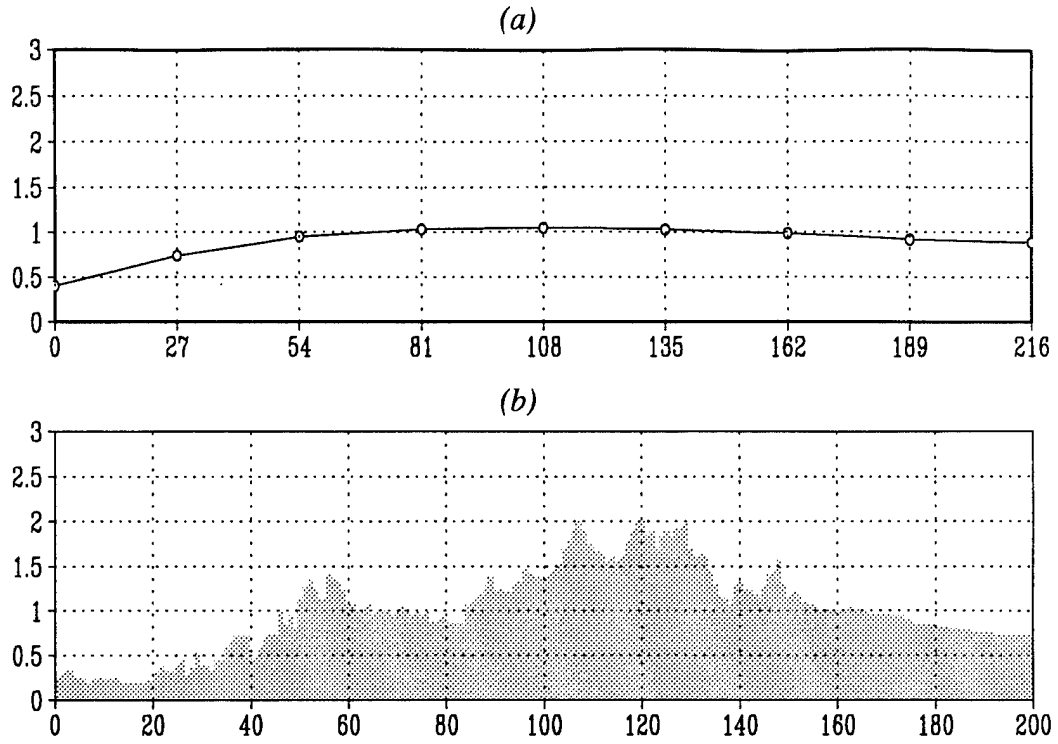

Figure 26. Comparison of terrain data along line AB for: (a) the 27 km MM5 model and (b) high-resolution DTED database.

b. Validation

1) RADAR DETECTION OF BIRDS

Due to the extreme sensitivity of the WSR-88D radar to clear-air returns, the detection of birds are a common occurrence. Battan (1973) notes several investigators who describe ring-shaped echoes that expand with time. Studies of simultaneous radar and visual observations confirmed that these donut echoes were composed of waves of birds flying away from nesting areas near sunrise. This type of signature was frequently observed on the WSR-88D radar at Wilmington, Ohio during the summer months of 1996.

Once such situation occurred on August 7, 1996. The region was dominated by high pressure with few clouds and areas of light fog or haze characterized by a stable

environment. The upper-air sounding and modified refractivity profile are shown in Figure 27. Although no surface duct is present, the layer between 400 and 700 meters is superrefractive. Also, a weak elevated duct exists at about 1750 meters. This environment suggests that atmospheric superrefraction or ducting may exist and allow long-range propagation and detection of targets not normally detectable.

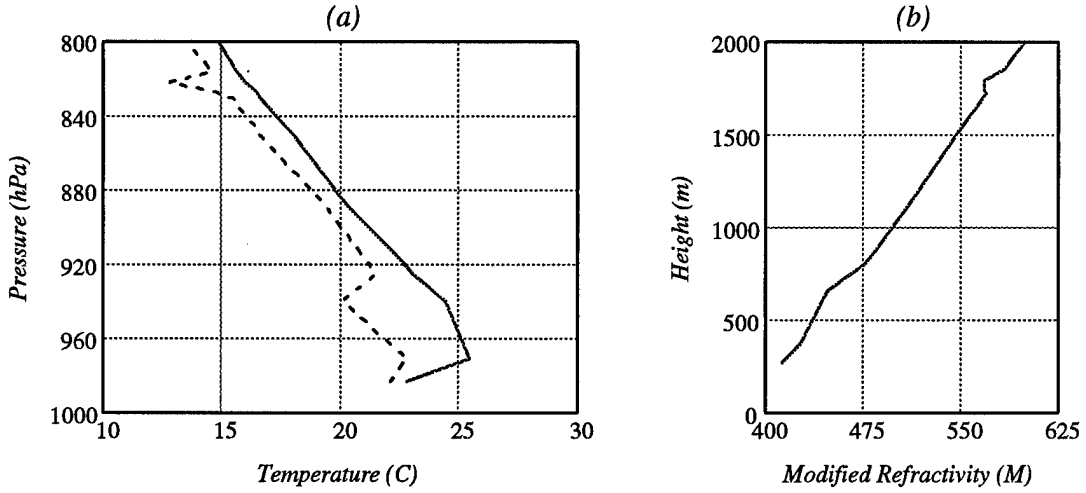

Figure 27. 12 UTC Radiosonde data and modified refractivity profile at Wilmington, OH on August 7, 1996. In (a) the solid line represents temperature and the dotted line is dewpoint.

Figure 28 shows a time sequence of base reflectivity as detected by the radar on August 7, 1996. A striking feature from this image is the detection of birds (indicated by the rings) at very long ranges away from the radar: Huntington, WV and Lexington, KY are about 160 km distant. At this range, the WSR-88D calculates from standard atmosphere the altitude of the detected targets to be about 12,000 feet (3.6 km). Clearly there must be a height error involved here since most birds do not fly at such altitudes. With the help of the VTRPE program, we can determine the magnitude of this height error.

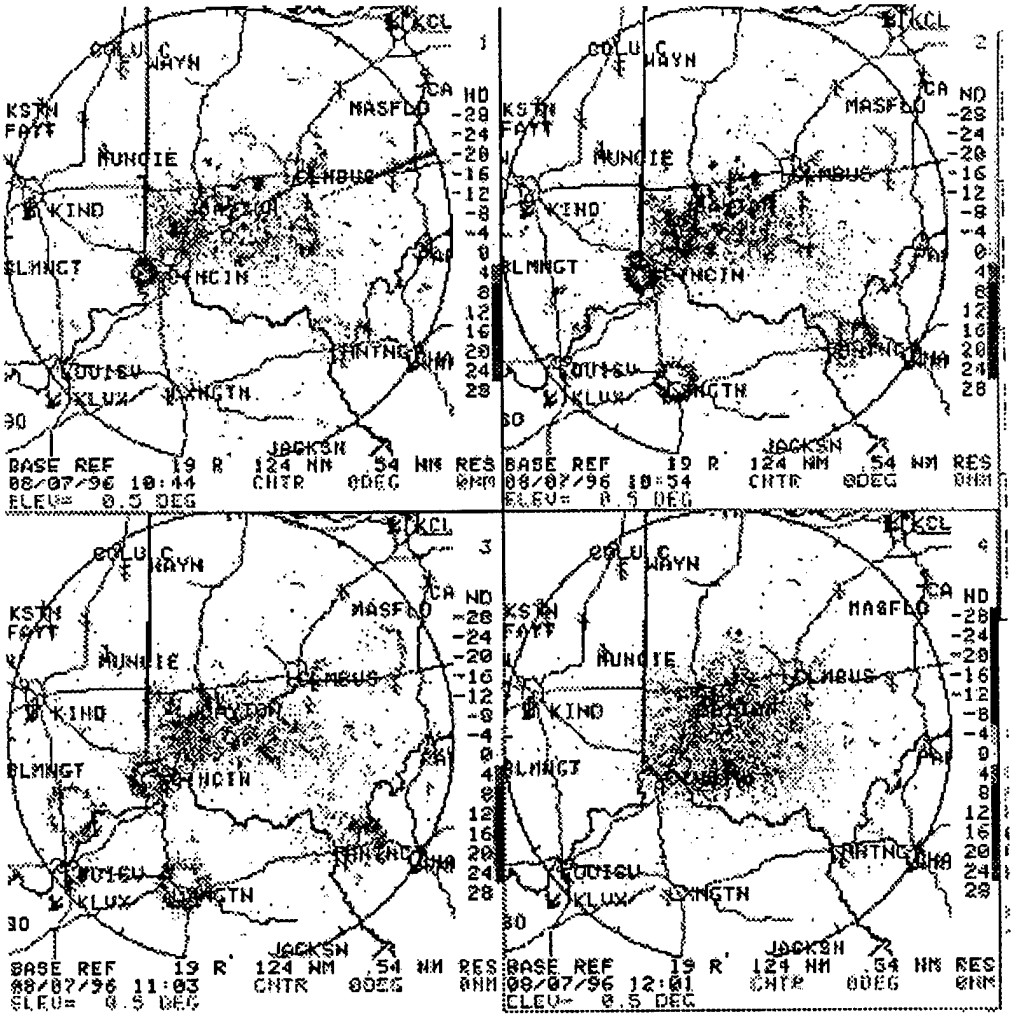

Figure 28. Time sequence of base reflectivity (0.5 degree) from the ILN WSR-88D radar on August 7, 1996: 10:44, 10:54, 11:03, and 12:01 UTC. Note the signature for sunrise indicated by the radial of enhanced reflectivity to the northeast (upper left). Expanding rings are probably birds flying out from nesting sites. The range ring marks 124 nmi (223 km) from the radar.

The maximum reflectivity return from the birds over Lexington, KY was a value of 16 dBZ. Since the conditions of Rayleigh scattering are clearly not met in this scenario[6],

[6] Bird targets may be approximated by a sphere of water whose mass is equal to that of the bird. For most birds this means a sphere radius of about 10 cm. For S-band radars, this target will scatter in the Mie regime.

this value of equivalent reflectivity is related to radar reflectivity factor (η) by the following equation (Sauvageot, 1992)

$$\eta = \frac{\pi^5 |K|^2}{\lambda^4} Z_e \tag{11}$$

where Z_e is the equivalent radar reflectivity determined from received signals in Figure 28, $|K|^2$ is the dielectric factor for liquid water, and λ is wavelength. This value for reflectivity factor can then be substituted in the following radar equation to determine the amount of power received at the radar

$$P_r = \frac{P_t g^2 \lambda^2 \theta^2 h \eta}{1024 \ln(2) \pi^2 r^2} \tag{12}$$

where P_t is the transmitted power, g is the antenna gain, λ is the transmitter wavelength, θ is the beamwidth, h is the pulse length, η is the reflectivity as calculated in Equation 11, and r is the range to the target. However, this calculation assumes that the target is at the center of the radar beam, which we have already determined is highly unlikely.

The method to include effects of propagation is to modify Equation 12 to include a 'pattern propagation factor', F (Craig and Levy, 1991; Kerr, 1951).

$$P_r = \frac{P_t g^2 \lambda^2 \theta^2 h \eta}{1024 \ln(2) \pi^2 r^2} F^4 \tag{13}$$

The pattern propagation factor, F, is calculated in the VTRPE program and is related to the propagation pathloss output (in dB) by the following equation (Ryan, 1991a)

$$PL = 20 \log\left(\frac{4\pi r}{\lambda F}\right) \tag{14}$$

With Equations 11 through 14, we can determine what maximum value of one-way propagation pathloss is allowable in order to detect the given target at a particular range.

For this example, a maximum pathloss value of 190 dB is allowed in order to detect this 16 dBZ_e target at 160 km where the minimum received power at the WSR-88D radar must be -113 dBm or greater.

Figure 29 shows the VTRPE generated radar coverage diagram of propagation pathloss for the standard atmosphere approximation and for August 7th. In a standard atmosphere a large region of greater than 210 dB pathloss exists beyond 100 km at lower elevations. On August 7th, pathloss in this region is decreased to 160-210 dB making targets there potentially detectable. These pathloss values calculated by VTRPE provide insight into the lowest possible altitude this radar can detect the bird targets detected in Figure 28.

In this case study, the 190 dB contour represents the maximum contour of probable target detection based upon the calculations in the previous paragraphs. The radar assumes that the target detected is in a standard atmosphere and is along the center of the main lobe of the radar beam. This places the birds at an altitude of 3.6 km (3.3 km above the ground), a highly unlikely altitude. From the VTRPE output (Figure 29b), the main 190 dB contour intersects the 160 km range at about 0.8 km altitude which is about 500 m above the ground. This represents the minimum altitude that the targets can be so that the radar can detect them. This altitude is a much more reasonable approximation that that of standard atmosphere.

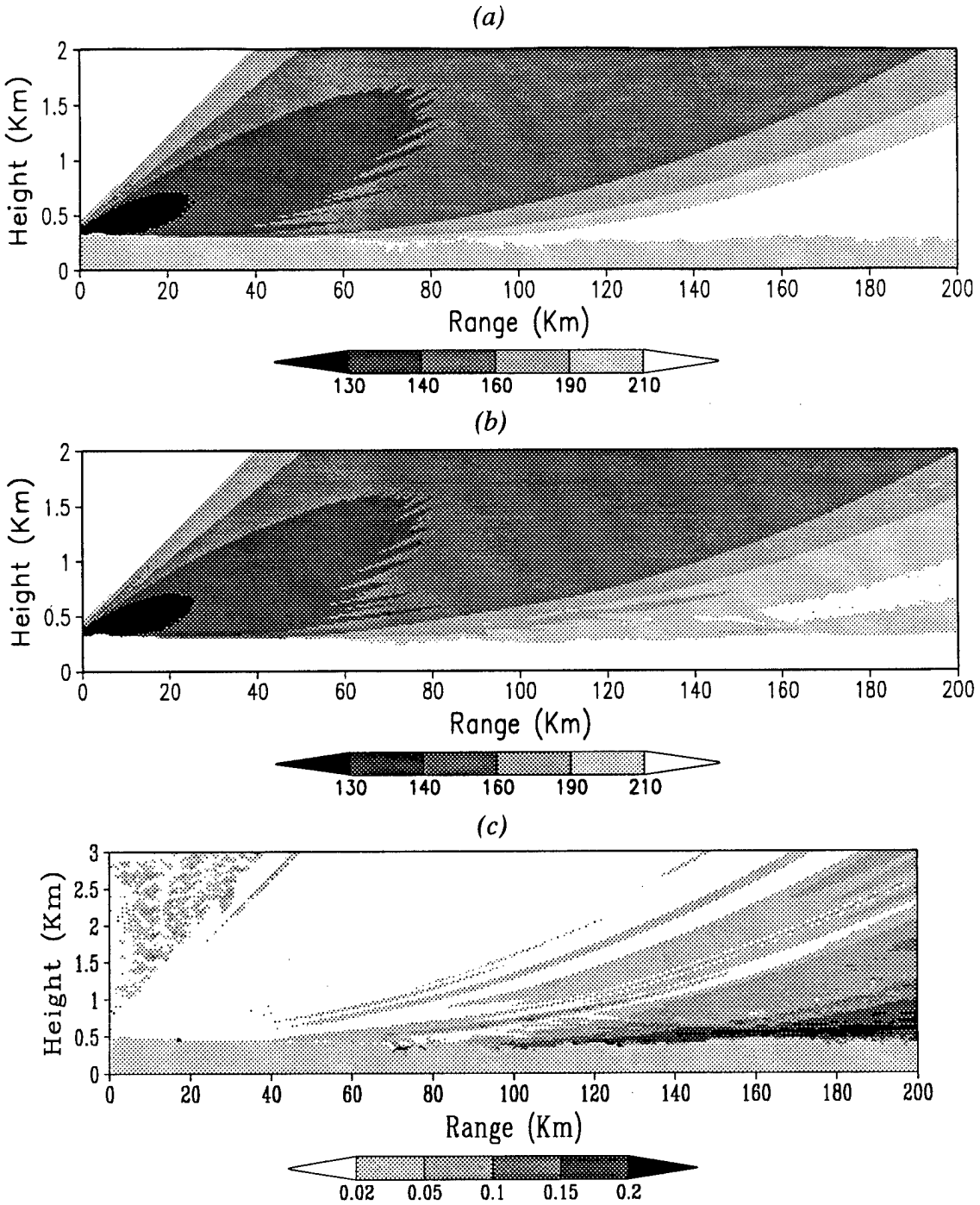

Figure 29. Radar coverage diagram of propagation pathloss (dB) for (a) standard atmosphere, and (b) on August 7, 1996 from Wilmington, OH to Lexington, KY. (c) is the error (%) in making a standard atmosphere assumption. The shaded region at the bottom in (a) and (c) indicates the ground

However, upon closer examination it is apparent that some energy is being ducted toward the earth's surface between 120 and 160 km. Between 150 and 160 km, where this energy is reflecting off the ground, there is a small region of minimal pathloss (160 to 190 dB) very close to the earth's surface. Based on these values, it is possible that the target is very close to the earth's surface, as we might expect birds to be.

Though this method does not give exact altitude, it does alert the radar operator that significant altitude errors do exist and that these targets are possibly at an altitude significantly lower than the assumed center of the radar beam.

2) HORIZONTAL VARIATION IN A "HOMOGENEOUS" ENVIRONMENT

One great advantage of the VTRPE program is that it allows for a horizontally variant atmosphere. Often, the assumption is made that the environment in the vicinity of a radar is horizontally homogeneous, or simply characterized by the nearest upper-air observing station. This is especially true if the radar is located over land with no significant variation in terrain or near large bodies of water. However, even in this situation, there may exist enough small-scale variation in the refractivity field that significant differences in the radar coverage occur. One such case occurred on October 5, 1996.

On this day, the atmosphere was very stably stratified with a cold front having passed through the day prior. Clear skies allowed for radiational cooling so that surface temperatures were low (near 0 °C) with a very strong surface inversion. Areas of patchy fog were reported, especially near bodies of water such as streams and lakes. In addition to the routine 12 UTC upper-air observation taken by the National Weather Service at

Wilmington (ILN), OH, two additional observations were taken to capture the horizontal stratification of the region. The two additional sites were located at Wright-Patterson AFB (FFO) and Circle Hill, OH which were 45 and 90 km respectively to the northwest of Wilmington.

Figure 30 shows the upper-air soundings at these locations on October 5, 1996. One noticeable difference between ILN and the other two sites is the data resolution. The two alternate sites used very high resolution instruments that sampled over 65 observations in the lower 2 km of the atmosphere. Compared to the 13 data points from the NWS observation, this resulted in a much finer picture of the small-scale variations in refractivity. In addition, the observations at FFO and Circle Hill had a much greater sensitivity to moisture than the NWS radiosonde. These two sites recorded two very dry layers at about 925 and 850 hPa that were not seen in the ILN sounding.

Figure 31 shows the corresponding modified refractivity profiles for the three locations. Only ILN and FFO showed the shallow evaporation duct near the earth's surface. The high-resolution soundings at FFO and Circle Hill detected an elevated duct between 700 and 750 meters that was detected in the ILN profile by a small superrefractive layer.

These three refractivity profiles were used in VTRPE to model the electromagnetic propagation of a radar and determine the significance of the two additional data points provided at FFO and Circle Hill. The atmosphere was first modeled as homogeneous using only the data from the NWS site at Wilmington. This result was compared to the coverage diagram using all three soundings.

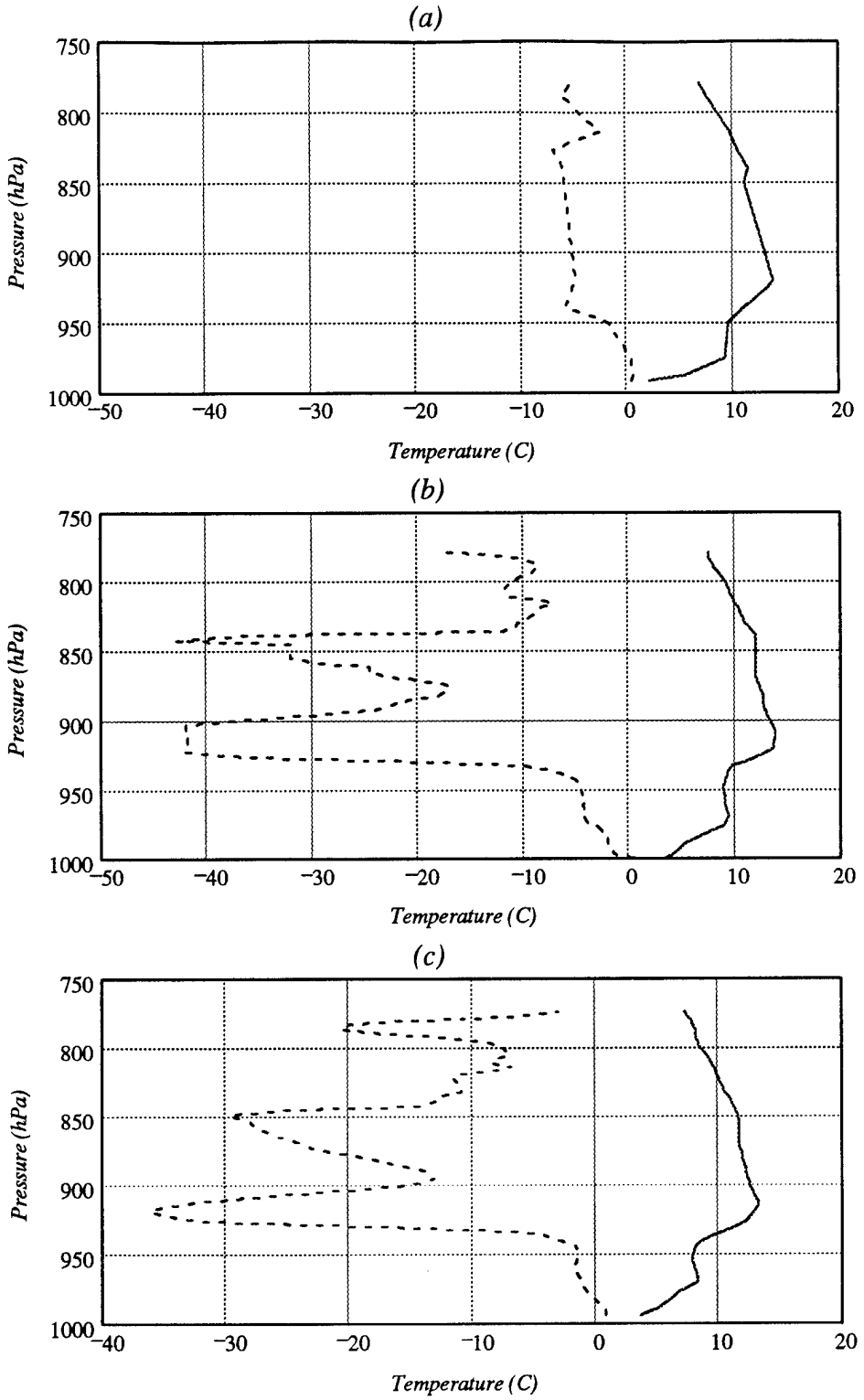

Figure 30. 12 UTC soundings for (a) Wilmington, (b) Wright-Patterson AFB, and (c) Circle Hill, OH on October 5, 1996. Plotted are temperature (solid) and dewpoint (dotted)

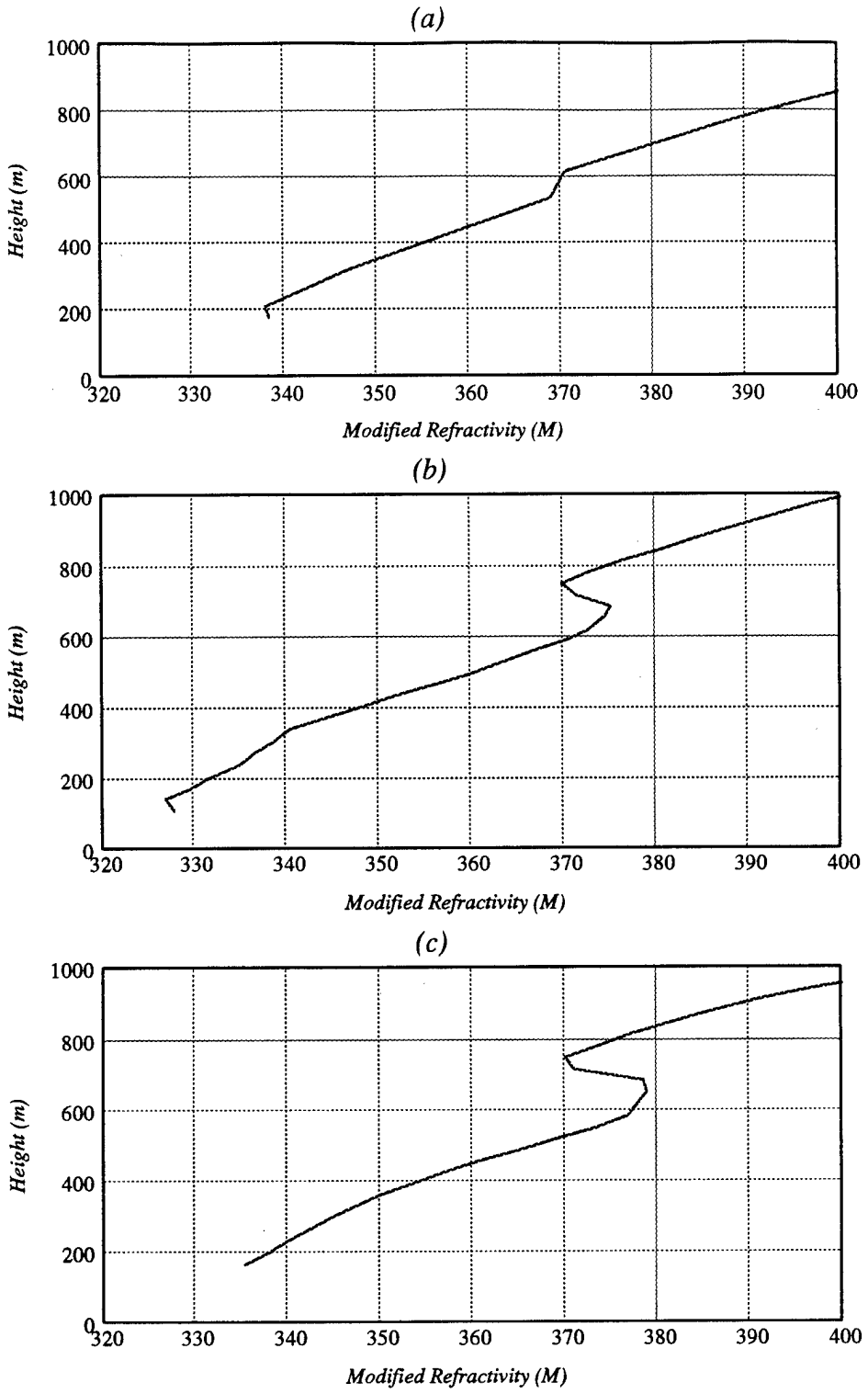

Figure 31. 12 UTC modified refractivity profiles for (a) Wilmington, (b) Wright-Patterson AFB, and (c) Circle Hill, OH on October 5, 1996.

The radar coverage diagrams of propagation pathloss is shown in Figure 32. With only the ILN sounding, the surface duct seen in Figure 32a is modeled to exist out to 200 km. As a result, a layer of 140-150 dB pathloss exists in the lowest 250 meters beyond about 80 km. When the additional sounding are included, this layer of lower pathloss values begins to lift beyond 100 km (Figure 32b). This is a result of the observation at Circle Hill which does not identify a surface ducting layer. Beyond 90 km, the radar energy is allowed to propagate more normally so that it increases in altitude.

Though the difference is subtle, the impact on military operations could be potentially more significant. As an example, suppose a particular aircraft were able to fly undetected through regions of propagation pathloss as low as 150 dB. Under the "homogeneous" atmosphere, this aircraft could fly undetected at an altitude of 250 m to a range of about 100 km from the radar. If, however, the atmosphere is not assumed homogeneous and all soundings are used, this same aircraft would be detected as far as 160 km away from the radar, a 60% increase in detection range.

This example demonstrates the importance of using multiple soundings in the calculation of electromagnetic propagation. Even in the simplest of environments there exist enough small-scale variations in the refractivity field that important distinctions arise between a "homogeneous" and non-homogeneous simulation.

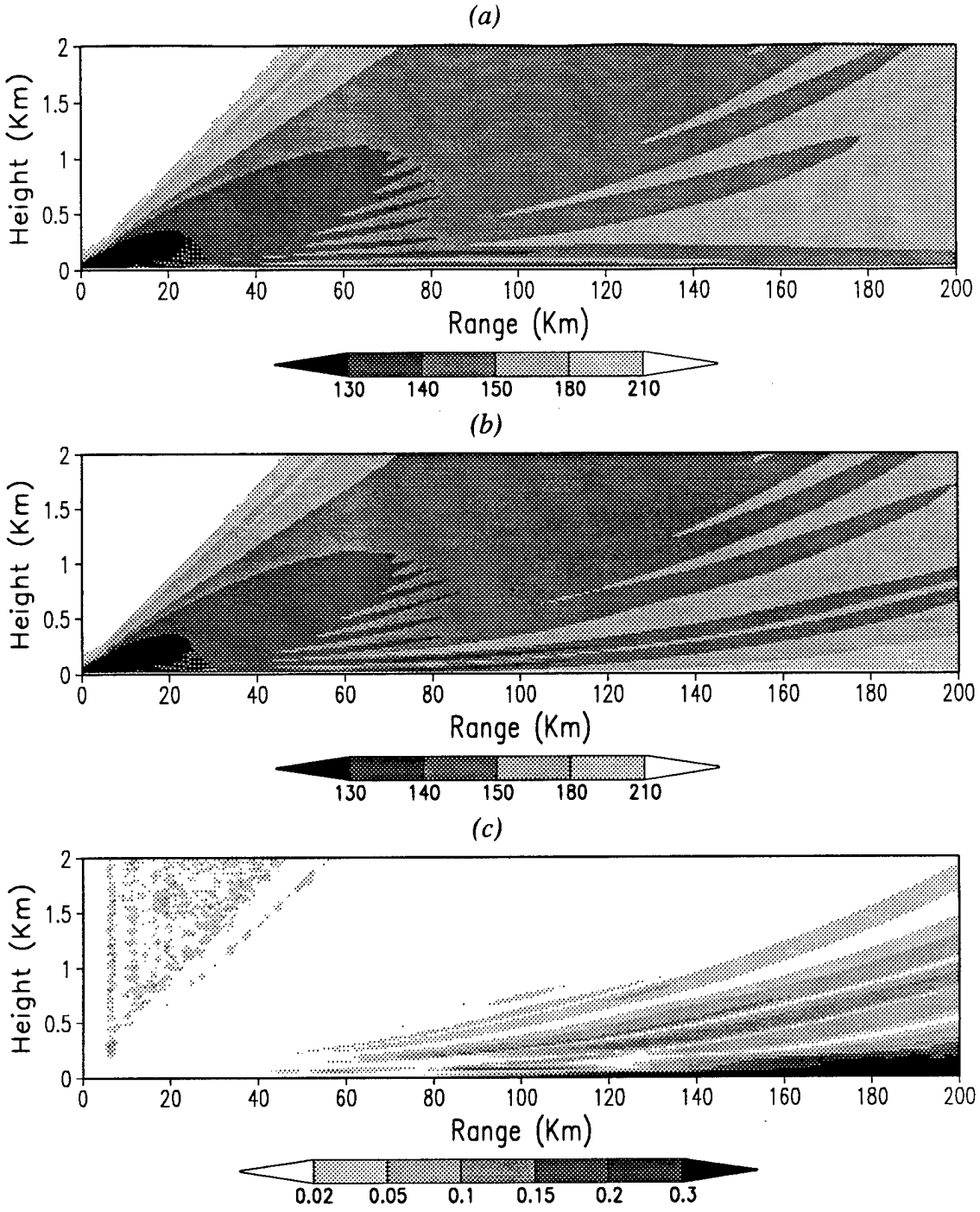

Figure 32. Radar coverage diagrams of propagation pathloss (dB) on October 5, 1996. In (a) a homogeneous atmosphere is assumed using sounding data only from ILN. In (b) the atmosphere is treated inhomogeneous using data from all three locations. (c) shows the error (%) in making a homogeneous atmosphere assumption.

Chapter 5. Conclusion and Recommendations

VTRPE is a powerful and flexible program that provides accurate calculations of the radar propagation conditions of the atmosphere. It is limited however, by the accuracy and resolution of the input data. The main purpose of this study was to quantify the sensitivity of the VTRPE propagation model to the accuracy and resolution of the atmospheric parameters that go into calculation of refractivity. Additionally, two case studies were examined to test the utility of VTRPE in operational use.

a. Sensitivity.

One might expect the errors in calculating the propagation pathloss of radio-wave energy to increase with increasing measurement error of the meteorological parameters. This was the case when these errors were treated independently. However, when errors of all parameters (pressure, temperature, and humidity) were included in the calculation, the error in pathloss calculation was nearly constant.

When errors were treated independently, it was found that this sensitivity was dependent, in part, upon the environment in which the radar is operating. In the standard and subrefractive environments, the VTRPE model showed a substantially greater sensitivity to measurement of humidity than pressure or temperature alone. Average RMSE errors in pathloss calculation ranged from 1.5% to over 5% when the maximum error in measuring humidity increased from 1% to 5%. However, when a propagation duct was present (either surface or elevated) the VTRPE program did not exhibit a significantly greater sensitivity to any one of the parameters alone. In an elevated duct

environment, the average RMSE values for the three parameters ranged from near 1.5% at error level 1 to around 2.8% at error level 5. With an evaporation duct, the errors ranged from 1.3% to near 2%.

When errors in measuring pressure, temperature, and humidity were all included in the model, the average RMSE was relatively constant at around 1.8% for the standard, subrefractive, and evaporation ducting atmospheres. In the elevated ducting atmosphere this value was slightly higher at 2.2%.

Whether or not these errors are acceptable is largely a matter of user requirements and also depends greatly on the radar and the type of target. Although the average RMSE errors ranged from only 0.5% to as much as 5%, the errors in pathloss calculation could be much higher in particular regions. Most of the error in VTRPE generated radar coverage diagrams was less than 2%. However, much higher errors existed at low elevations and long distances from the radar. The region below 500 meters elevation at 100 km range and beyond was characterized by a 2-5% error in pathloss calculation with scattered areas of 5-10%. Depending on the target and the radar sensitivity, the errors at this range may mean the difference between detection or non-detection.

Though some may argue that improving instrument accuracy will produce better results from VTRPE, this does not seem to be the case here. The RMSE results remained relatively constant regardless of the level of error input into the parameters. What is important, however, is the frequency with which sounding observations are measured; the vertical resolution. It is critical to record many observations of the lower atmosphere to capture the small scale variations in refractivity. This difference was evident on

October 5, 1996 (see Figure 30 and Figure 31 on pages 62-63) when comparing results from the lower resolution NWS radiosondes with the high-resolution sondes used by the military.

VTRPE was not very sensitive to changes in model resolution when using the MM5 27 km mesoscale model data for input. Comparisons between 54 km resolution data with 27 km resolution showed relatively minor changes in pathloss calculations by VTRPE. Overall, using 54 km data resulted in less than 2% error from using the 27 km data. Only two small regions had differences greater than 2%. When resolution was reduced down to 81 km, no significant additional error in pathloss calculation resulted. This suggests that an 81 km model may be sufficient to generate propagation predictions using VTRPE. However, this could also suggest that the 27 km model itself does not accurately model the horizontal variations of refractivity across a marine boundary layer and is not significantly better than an 81 km model.

Also, this study uncovered a difficulty when using numerical model data for inputs into VTRPE. The terrain used in the atmospheric model is a much coarser terrain than would be used by operational users of the VTRPE program. Errors can result when the lower-resolution terrain in the model atmospheric profiles do not match with the high-resolution terrain used in the VTRPE program itself. If a computer model is to be any good at capturing the horizontal variations of refractivity it needs also to use high resolution terrain.

Similarly, VTRPE was not significantly sensitive to changes in the vertical resolution of data although it was slightly more so than to changes in horizontal

resolution. Reducing the number of data levels from 55 to 28 resulted in less than a 2% error over most of the coverage diagram. Regions in the shadow of mountain peaks had higher errors in the range 2-5% while the region just above the main radar beam was as high as 20% in error. When the vertical resolution was reduced down to 18 levels, no significant additional error in pathloss calculation resulted.

This could suggest one of two conclusions. Either an 18 level model could be adequate to forecast propagation conditions or the 55 level model itself is not adequate enough. These results could also change based upon the exact location of the sample of data. This analysis only sampled a small cross-section of a complicated maritime/continental environment.

b. Validation.

The VTRPE model demonstrated usefulness in determining possible height errors in the detection of birds flying away from their nesting sites at sunrise. On August 7, 1996, a WSR-88D weather radar detected several bird echoes at very long ranges. A maximum pathloss value was calculated using the generalized radar equation and information from the base reflectivity product of the radar. From a radar coverage diagram generated by the VTRPE model, it was determined that these echoes possibly could have been near the earth's surface rather than at the radar-calculated height of over 3 km.

Another case of anomalous propagation was observed on October 5, 1996. On this day, three radiosonde observations were available to provide more accurate representation of the atmosphere. On this day, all three points of data were important in accurately modeling the propagation conditions within the range of the radar. Even in the

supposedly horizontally homogeneous region of southwestern Ohio enough horizontal variations do exist to present significant differences when using VTRPE to model radar propagation. In this case as much as 30% error would have resulted when approximating the real atmosphere as homogeneous.

c. Suggestions for future investigation.

Many different parameters exist in the calculation of refractivity and pathloss using the VTRPE computer program. This paper only investigated the effects on an S-band (3 GHz) radar. Different results may occur at other frequencies and with other radar types.

Also, the sensitivity study was only a partial statistical analysis of the effects of pressure, temperature, and humidity on calculating pathloss. A more thorough multivariate statistical study of the complex interactions of these parameters may provide further insights into their correlation.

Since the 27 km model used in this study did not show significant horizontal variations of refractivity, an even higher resolution model might provide better results. Likewise, a model with more than 55 levels or with a greater concentration in the lower elevations might capture more of the fine variations in refractivity. Earlier, it was suggested that the atmosphere in the immediate vicinity of the radar was more critical in pathloss calculations than any other region of the environment. If this is true, it is more critical to get an accurate, high-resolution refractivity profile at the radar itself than to increase the number of vertical profiles used in the VTRPE program.

Appendix A: Propagation Modeling and the Parabolic Equation

a. Background

Several methods of modeling electromagnetic wave propagation have been developed in recent years: geometric optics, mode theory, and the parabolic equation. Geometric optics is useful for describing simple cases of atmospheric refractivity conditions utilizing simple ray tracing and Snell's law. However, Craig (1988) notes that while ray tracing provides reasonable qualitative results, it is far too difficult to use when quantitative analysis is desired. Some other difficulties are:

- Interference and wave interaction are not easily evaluated.
- Propagation loss and diffraction phenomena are not accounted for.
- It does not allow for horizontal variations in the refractive index structure.
- The assumptions of geometric optics become invalid when strong refractive gradients are encountered.

As a result, engineers turned to physics, numerical methods, and mode theory to more accurately solve this problem. This method involves direct solution of Maxwell's equations for the electromagnetic field where the troposphere is modeled analogous to a dielectric-filled waveguide. However, computational analysis of this method is only practical assuming a horizontally homogeneous atmosphere for very simplified refractivity profiles. Though this method is useful for very long ranges, it is not practical to capture the small-scale interference often seen in radar coverage diagrams. Also, a full two-dimensional, range-height picture of radar coverage is extremely expensive to produce (Craig and Levy, 1991).

In 1946, Leontovich and Fock introduced the parabolic wave equation as a simplified version to the full-wave approach to solving radiowave propagation in the troposphere. However, it has not been until recent advances in numerical methods and computer power that the use of this method has become successful. Taking advantage of the fast Fourier transform method, Hardin and Tappert (1973) developed the split-step Fourier parabolic equation algorithm and applied it to modeling ionospheric radar propagation. According to Barrios (1992) the Fourier split-step algorithm has two advantages: (1) it provides an exact solution to the electromagnetic field equations, and (2) it can predict the electromagnetic field in an environment that is both horizontally and vertically inhomogeneous. In 1977, Tappert successfully implemented this method for the case of acoustic wave propagation in the ocean. In 1983, Ko et al. used the parabolic equation and the split-step method to examine the detailed effects of refractivity gradients on microwave propagation.

The great advantage of using the parabolic equation is that it overcomes the severe limitations of ray and mode theory. It also allows rapid computation of a two-dimensional radar coverage diagram without making unrealistic assumptions about the atmosphere (Craig and Levy, 1991).

b. The Parabolic Equation

The first step in deriving the parabolic equation is to derive a vector wave equation from Maxwell's equations of electromagnetic radiation. This equation is

$$\frac{\partial^2 \Psi}{\partial z^2} + \frac{\partial^2 \Psi}{\partial x^2} + k^2 n^2 \Psi = 0 \qquad \text{(A1)}$$

where $\Psi(x,z)$ is the electromagnetic field component, $k = 2\pi/\lambda$ is the free space wave number , and $n(x,z)$ is the refractive index (Craig and Levy, 1991). By converting to spherical coordinates, applying an earth-flattening transformation, and assuming azimuthal symmetry about the radar, Equation A1 can be written

$$\frac{\partial^2\Psi}{\partial z^2} + \frac{\partial^2\Psi}{\partial x^2} + \frac{1}{x}\frac{\partial\Psi}{\partial x} + k^2 M^2(x,z)\Psi = 0 \qquad \text{(A2)}$$

where M is the modified index of refraction as defined in Chapter 2 of this paper.

The parabolic approximation takes advantage of the fact that the variations of the refractivity field occur on a scale much larger than the frequency of the electromagnetic wave energy. With this assumption the field component Ψ can then be expressed in terms of an attenuation function $u(x,z)$,

$$\Psi(x,z) \approx u(x,z)\cdot e^{ikx}(x)^{-1/2}, \qquad \text{(A3)}$$

where the attenuation function acts to remove the rapid phase variation of the field. Assuming that we are interested in solutions at a large number of wavelengths distant from the source, and that u is slow to vary, u satisfies a parabolic equation:

$$\frac{\partial^2 u}{\partial x^2} + 2ik\frac{\partial u}{\partial x} + k^2\left(M^2(x,z) - 1\right)u \approx 0, \qquad \text{(A4)}$$

where modified refractivity can be a function of both height z, and range x. Thus, given the range-height distribution of refractivity, we can compute the attenuation function. With the attenuation function, the electromagnetic field can be computed from Equation A3.

Appendix B: Computation of Refractivity Values

Calculation of refractivity (N) begins with the equation relating refractivity to the commonly measured meteorological parameters of pressure, temperature, and vapor pressure:

$$N = \frac{77.6}{T}\left(p + 4810\frac{e}{T}\right). \tag{B1}$$

Vapor pressure (e) is a function only of dewpoint and is given by Teten's formula,

$$e = 6.11 \cdot 10^{\left(\frac{aT_d}{b+T_d}\right)}, \tag{B2}$$

where T_d is in Celsius and vapor pressure is given in hPa (Bolton, 1980). The values for constants a and b are listed in Table B1. The saturation vapor pressure can be calculated using Equation B2 using temperature (in °C) instead of dewpoint.

Table B1. Values of constants a and b in Equation B2

	a	b (K)
$T_d > 0$ C	7.5	237.3
$T_d \leq 0$ C	9.5	265.5

Refractivity is converted into modified refractivity by the equation,

$$M = N + \left(h/a\right) \cdot 10^6 \tag{B3}$$

where h is the height and a is the radius of the earth (6370 km). Height is calculated using the hypsometric equation,

$$h = h_0 + \frac{R_d \overline{T}_v}{g_0} \ln\left(\frac{p_0}{p}\right) \tag{B4}$$

where $\overline{T}_v$ is the mean virtual temperature between two layers and g_0 is the acceleration due to gravity at the earth's surface ($9.81\ m\ s^{-2}$), and h_0 and p_0 are the height and pressure of some reference level. The virtual temperature is given by the relationship,

$$T_v = T\left(1 - 0.378\frac{e}{p}\right)^{-1}. \tag{B5}$$

Given a typical radiosonde profile of pressure, temperature, and dewpoint, the refractivity (N) and modified refractivity (M) are readily calculated using Equations B1 - B5.

The Standard Atmosphere

The temperature profile of a standard atmosphere in the lowest 10 km is closely approximated by a linear decrease of 6.5° C km^{-1} and an exponential decrease in pressure. From the hydrostatic approximation and ideal gas law, pressure as a function of height is given by,

$$p(z) = p_0 \cdot \exp\left(\frac{-z}{H}\right) \tag{B6}$$

where H is the scale height ($H = {}^{R_d T}/_{g_0}$) and p_0 is usually taken to be 1013.25 hPa. Humidity is defined as the ratio of vapor pressure to saturation vapor pressure, $RH = {}^{e}/_{e_s}$. From these equations, values of refractivity can be computed for varying degrees of humidity (e.g. see Figure 1 and Figure 2 on pages 9-10).

Table B2 lists the values of refractivity and modified refractivity in the lowest 10 km of the troposphere for varying degrees of humidity in a standard atmosphere.

Table B2. Refractivity (*N*) and modified refractivity (*M*) values for a standard atmosphere with selected relative humidities.

Altitude	RH=0%		RH=30%		RH=60%		RH=100%	
(Km)	N	M	N	M	N	M	N	M
0	272.9	272.9	296.2	296.2	319.2	319.2	349.6	349.6
1	247.3	404.3	263.1	420.1	278.8	435.8	299.5	456.5
2	222.9	536.9	233.4	547.4	243.9	557.8	257.7	571.7
3	199.8	670.8	206.4	677.3	212.9	683.8	221.5	692.5
4	178.1	806.0	182.0	809.9	185.8	813.8	191.0	818.9
5	157.7	942.6	159.9	944.8	162.1	947.1	165.1	950.0
6	138.6	1080	139.9	1082	141.1	1083	142.8	1085
7	120.9	1220	121.6	1221	122.3	1221	123.2	1222
8	104.6	1361	105.0	1361	105.3	1361	105.8	1362
9	89.7	1503	89.9	1503	90.1	1503	90.3	1503
10	76.2	1646	76.3	1646	76.4	1646	76.5	1646

Bibliography

Barrios, A. E., 1992: Parabolic equation modeling in horizontally inhomogeneous environments. *IEEE Trans. Antennas Propag.*, **40**, 791-797.

Battan, L. J., 1973: *Radar Observation of the Atmosphere*. Univ. of Chicago Press, 324 pp.

Bean, B. R. and E. J. Dutton, 1966: *Radio Meteorology*. Natl. Bur. Stand. Monogr. 42, U. S. GPO, 435 pp.

Bolton, D., 1980: *The computation of equivalent potential temperature*, Mon. Wea. Rev., **108**, 1046-1053.

Bluestein, Howard B., 1993: *Synoptic-Dynamic Meteorology in Midlatitudes, Vol. 2*. Oxford University Press, 594 pp.

Cook, J., 1991: A sensitivity study of weather data inaccuracies on evaporation duct height algorithms. *Radio Sci.*, **26**, 731-746.

Craig, K. H. and Levy, M. F., 1991: Parabolic equation modeling of the effects of multipath and ducting on radar Systems. *IEEE Trans. Antennas Propag.*, **138**, 153-162.

Craig, K. H., 1988: Propagation modeling in the troposphere: parabolic equation method. *Electronics Letters*, **24**, 1136-1139.

Dockery, G. D., 1988: Modeling electromagnetic wave propagation in the troposphere using the parabolic equation. *IEEE Trans. Antennas Propag.*, **36**, 1464-1470.

Dockery, G. Daniel and Gerald C. Konstanzer, 1987: Recent advances in prediction of tropospheric propagation using the parabolic equation. *Johns Hopkins APL Tech. Dig.*, **8**, 404-412.

Fleagle, R. G. and J. A. Businger, 1980: *An Introduction to Atmospheric Physics*. Academic Press, 432 pp.

Gossard, E. E., 1978: The height distribution of refractive index parameter in an atmosphere being modified by spatial transition at its lower boundary. *Radio Sci.*, **13**, 489-500.

Hardin, R. H. and F. D. Tappert, 1973: Application of the split-step Fourier method to the numerical solution of nonlinear and variable coefficient wave equations. *SIAM Review*, **15**, 423.

Hitney, H. V., and J. H. Richter, 1976: Integrated Refractive effects Prediction System (IREPS), *Nav. Eng. J.*, **88**, 257-262.

Hitney, H. V., J. H. Richter, R. A. Pappert, K. D. Anderson, and G. B. Baumgartner, Jr., 1985: Tropospheric radio propagation assessment. *Proc. IEEE*, **73**, 265-285.

Kerr, D. E., 1951: *Propagation of Short Radio Waves*. McGraw-Hill, 728 pp.

Ko, Harvey, James Sari, and Joseph Skura, 1983: Anomalous microwave propagation through atmospheric ducts. *Johns Hopkins APL Tech. Dig.*, **4**, 12-26.

Paulus, Richard A., 1994: VOCAR: An experiment in variability of coastal atmospheric refractivity. Proc. IGARSS '94, 386-388.

Rinehart, Ronald E., 1991: *Radar for Meteorologists*. Rinehart, 334 pp.

Rogers, L. Ted., 1996: Effects of the variability of atmospheric refractivity on propagation estimates. *IEEE Trans. Antennas Propag.*, **44**, 460-465.

Ryan, Frank J., 1991a: *Analysis of electromagnetic propagation over variable terrain using the parabolic wave equation*. TR1453, Naval Ocean Systems Center, San Diego, 38 pp.

-----, 1991b: *User's guide for the VTRPE computer model*. TR1456, Naval Ocean Systems Center, San Diego, 51 pp.

Schemm, C. E., L. P. Manzi, and H. W. Ko., 1987: A predictive system for estimating the effects of range- and time-dependent anomalous refraction on electromagnetic wave propagation. *Johns Hopkins APL Tech. Dig.*, **8**, 394-403.

Tappert, F. D., 1977: The parabolic approximation method. *Wave Propagation and Underwater Acoustics*, J. B. Keller and J. S. Papadakis, Eds. Springer-Verlag, 224-287.

Wallace, J. M. and P. V. Hobbs, 1977: *Atmospheric Science, An Introductory Survey*. Academic Press, 467 pp.

Wilks, Daniel S., 1995: *Statistical Methods in the Atmospheric Sciences*. Academic Press, 467 pp.

Vita

Captain Matthew K. Doggett was born on 24 August 1970 in Moses Lake, Washington. In 1988 he graduated from Wenatchee High School and began undergraduate studies at the University of Washington in Seattle with a four-year ROTC scholarship. In 1992 he graduated with a Bachelor of Science degree in Atmospheric Sciences and received his commission into the Air Force.

Prior to entering active duty, Capt Doggett served as a research assistant for the Atmospheric Sciences department at the University of Washington. He entered active duty in 1993 as a Wing Weather Officer at Mountain Home AFB, Idaho. As his second active duty assignment, in August 1995 he enrolled in the Meteorology program of the School of Engineering, Air Force Institute of Technology.

Permanent Address: 300 W. Penny Rd.
Wenatchee WA 98801

REPORT DOCUMENTATION PAGE

Form Approved
OMB No. 0704-0188

1. AGENCY USE ONLY (Leave blank)	2. REPORT DATE	3. REPORT TYPE AND DATES COVERED
	March 1997	Master's Thesis, Final

4. TITLE AND SUBTITLE
An Atmospheric and Sensitivity Study of the Variable Terrain Radio Parabolic Equation Model

5. FUNDING NUMBERS

6. AUTHOR(S)
Matthew K. Doggett, Captain, USAF

7. PERFORMING ORGANIZATION NAME(S) AND ADDRESS(ES)
AFIT/ENP
2950 P. Street, Bldg 640
WPAFB, OH 45433-7765

8. PERFORMING ORGANIZATION REPORT NUMBER
AFIT/GM/ENP/97M-04

9. SPONSORING/MONITORING AGENCY NAME(S) AND ADDRESS(ES)
88 WS.
2049 Monahan Way, Bldg 91
WPAFB, OH 45433
Attn: Capt. Dave Wood

10. SPONSORING/MONITORING AGENCY REPORT NUMBER

11. SUPPLEMENTARY NOTES

12a. DISTRIBUTION/AVAILABILITY STATEMENT
Approved for public release; distribution unlimited

12b. DISTRIBUTION CODE

13. ABSTRACT (Maximum 200 words)

The Variable Terrain Radio Parabolic Equation (VTRPE) computer model is a powerful and flexible program that provides calculations of the radar propagation conditions of the atmosphere. This study quantifies the sensitivity of the VTRPE model to the accuracy and resolution of the atmospheric parameters that go into it. Also, two case studies are examined to test the utility of VTRPE in operational use. Root Mean Squared Errors in propagation pathloss were calculated for four types of meteorological environments. While the overall RMSE averaged only 0.5% to 5%, in certain regions the errors in calculating pathloss were as high as 20%. VTRPE was used to calculate possible height errors when birds were detected at long ranges from a WSR-88D radar in a ducting environment. While the radar assumes a standard atmosphere when calculating height, results from VTRPE suggest that this resulted in possible height errors of over 3 km. Another case study of detected anomalous propagation was examined to determine the effects of multiple soundings in the VTRPE calculation of propagation pathloss. In this example, the effect of assuming a homogeneous atmosphere resulted in propagation pathloss errors of up to 30%.

14. SUBJECT TERMS	15. NUMBER OF PAGES
Radar, Radiowave Propagation, Modeling, Refractivity	93
	16. PRICE CODE

17. SECURITY CLASSIFICATION OF REPORT	18. SECURITY CLASSIFICATION OF THIS PAGE	19. SECURITY CLASSIFICATION OF ABSTRACT	20. LIMITATION OF ABSTRACT
Unclassified	Unclassified	Unclassified	UL